AD/A-003 690

# SEISMIC WAVE PROPAGATION AND EARTHQUAKE CHARACTERISTICS IN ASIA

C. Kisslinger, et al

Cooperative Institute for Research in Environmental Science

Prepared for:

Air Force Office of Scientific Research
Advanced Research Projects Agency

30 October 1974

# SEISMIC WAVE PROPAGATION AND EARTHQUAKE CHARACTERISTICS IN ASIA

C. Kisslinger, et al

Cooperative Institute for Research in Environmental Science

Prepared for:

Air Force Office of Scientific Research
Advanced Research Projects Agency

30 October 1974

UNCLASSIFIED

SECURITY CLASSIFICATION OF THIS PAGE (When Data Entered)

| REPORT DOCUMENTATION PAGE | READ INSTRUCTIONS BEFORE COMPLETING FORM |
|---|---|
| 1. REPORT NUMBER: AFOSR - TR - 74 - 1909 | 2. GOVT ACCESSION NO. |
| 3. RECIPIENT'S CATALOG NUMBER: AD/A-003690 | |
| 4. TITLE (and Subtitle): SEISMIC WAVE PROPAGATION AND EARTHQUAKE CHARACTERISTICS IN ASIA. | 5. TYPE OF REPORT & PERIOD COVERED: Final technical report 1 April-30 September, 1974 |
| | 6. PERFORMING ORG. REPORT NUMBER |
| 7. AUTHOR(s): C. Kisslinger, E. R. Engdahl, G. Boucher, and R. Ganse | 8. CONTRACT OR GRANT NUMBER(s): F44620-74-C-0015 |
| 9. PERFORMING ORGANIZATION NAME AND ADDRESS: CIRES, University of Colorado, Boulder, Colorado, 80302 | 10. PROGRAM ELEMENT, PROJECT, TASK AREA & WORK UNIT NUMBERS: ARPA ORDER 1827, Program Code 4F10, Program Element 62701E |
| 11. CONTROLLING OFFICE NAME AND ADDRESS: Advanced Research Projects Agency, 1400 Wilson Boulevard, Arlington, VA 22209 | 12. REPORT DATE: 30 October 1974 |
| | 13. NUMBER OF PAGES: 72 |
| 14. MONITORING AGENCY NAME & ADDRESS (if different from Controlling Office): Air Force Office of Scientific Research/NP, 1400 Wilson Boulevard, Arlington, VA 22209 | 15. SECURITY CLASS. (of this report): UNCLASSIFIED |
| | 15a. DECLASSIFICATION/DOWNGRADING SCHEDULE |

16. DISTRIBUTION STATEMENT (of this Report)

Approved for public release; distribution unlimited.

17. DISTRIBUTION STATEMENT (of the abstract entered in Block 20, if different from Report)

18. SUPPLEMENTARY NOTES

19. KEY WORDS (Continue on reverse side if necessary and identify by block number)

Focal mechanisn s
P residuals
Long-period body waves
Focal depth
Earthquake spectra



20. ABSTRACT (Continue on reverse side if necessary and identify by block number)

Refraction through the subducted plate distorts focal mechanism solutions of island are earthquakes. Source-related P- residuals show that the Hindu Kush seismic zone lies in a planar zone of high-velocity material. Multiplication of vertical and radial components of long-period body-waves improves detectability for smaller events. Source spectra for 12 mid-Asian events have been calculated from combined long-and short-period data.

DD FORM 1 JAN 73 1473 EDITION OF 1 NOV 65 IS OBSOLETE

UNCLASSIFIED

SECURITY CLASSIFICATION OF THIS PAGE (When Data Er

TABLE OF CONTENTS

## Technical Report Summary

Research on the effects of upper mantle structure in subduction zones has been directed toward two principal problems: the effects of plate structure on earthquake focal mechanism solutions and the use of carefully analyzed station residuals to reveal details of upper mantle structure.

Because of refraction effects, the point on the focal sphere corresponding to the ray to a seismograph station will be plotted in the wrong place if that ray has gone through a high velocity subducted slab, but a spherical earth model is used to determine the ray path. The size of the effect depends on the geometry of the source-slab-station system. For the Aleutian Islands event studied, changes in take-off angle of up to 8° and 19° in azimuth were produced by this effect. One conclusion for this particular event is that the newly calculated slip vector was concordant with accepted relative motion of the Pacific and North American plates. There is no need to postulate a separate Bering plate, as has been done by others on the basis of the systematic misfit of the slip vectors calculated by conventional methods.

Station P- time residuals have been systematically evaluated as a means of developing some detailed information on lateral variations in the crust and upper mantle of the Hindu Kush

seismic zone. All events occurring in this region and a nearby source in India, as reported by the ISC for 1964-70, were sorted by recording station and by source region within the overall zone. The residuals were then examined for degree of scatter and stability of mean residuals at individual stations as functions of space and time. Stations exhibiting stable means were plotted on a residual-sphere to look for evidence of significant patterns. Effects beneath the stations were removed by subtracting from the Hindu Kush residuals either the "normal" Indian source residuals or station corrections independently determined from deep-focus events (> 300 km). By both methods the residual-sphere plots suggest that the Hindu Kush seismic zone lies in a planar zone of high-velocity material, possibly a fossil plate, extending beneath the Hindu Kush source (~ 210 km) and dipping steeply to the northwest.

The development of techniques for improving the detectability of long-period body waves from Asian earthquakes as small as $m_b$ 5 and explosions with $m_b$ 6 or smaller has been the principal objective of current work on long-period body waves. Arrival-times and frequency content of HGLP signals can be derived from raw data with signal-to-noise ratios less than 1. Multiplication of vertical and phase-shifted radial components

of ground motion has been demonstrated to be an effective means for improving the signal to-noise ratio.

A deep, small earthquake produces a seismogram with a P- wave arrival and weak surface waves. If the depth of such an event is erroneously determined to be shallow, the event may be misidentified as an explosion on the basis of the $Ms/m_b$ criterion. Arrival-times of long-period S waves derived from processed HGLP data can be used to supplement the data set and produce a more nearly correct depth and origin time, thereby eliminating the event as a possible explosion. One case of an event that was actually at a depth of 350-400 km, but erroneously reported as being at 55 km illustrates this point. The validity of the procedure was subsequently verified on the basis of the arrival-times of one well-developed phase, PKP, that had been thrown out of the determination because it didn't fit the shallow depth.

The work on establishing a classification scheme for central Asian earthquakes has been handicapped by the sparsity of suitable data for studying events over a wide range of magnitudes within selected seismic zones. Recently seismograms of good quality from the Soviet observatory network have been obtained through World Data Center A, and these will make more complete studies possible.

Combined long-and short-period spectra from WWSSN seismograms for the following crustal events, by seismic region, have been calculated: (1) Tien-Shan (China-U.S.S.R. border region), 4 events, $m_b$ 5.7-6.2; (2) Tibet, 3 events, $m_b$ 5.6-5.8; (3) Tsaidam, 3 events, $m_b$ 5.2-6.1; Lake Baikal, 2 events, $m_b$ 5.1. The Lake Baikal events do not produce detectable P- signals on the long-period WWSSN seismograms. Preliminary examinations of the spectra reveals that the Tibetan source yields spectra with a single, well-developed corner period, whereas the Tien-Shan P- wave spectra suggest two corner frequencies, corresponding to a small fractional stress drop.

## 1. Effects of Plate Structure on the Determination of Earthquake Focal Mechanisms

E. R. Engdahl

The existence of a subducted plate beneath an island arc often makes it difficult for geophysicists to study seismic sources in these regions. The effects of pronounced lateral heterogeneity in physical properties on the seismic signal have been discussed by numerous authors (Jacob, 1972; Davies & Julian, 1972; Sleep, 1973). Engdahl (1973, 1974) considered the effects on earthquake hypocenters by allowing for plate structure in the location process rather than assuming that the Earth is laterally homogeneous.

This note was inspired by the observation that under certain circumstances of station geometry with respect to the seismic source the strike of either one or both of the nodal planes determined with a conventional Earth model may be significantly in error in the presence of a subducted plate. In the Aleutian arc a systematic error in the slip vectors is observed, producing some difficulty in modelling relative plate motions (Minster, et al, 1974).

The central Aleutians is an ideal place to model a subducted plate because of the data from large nuclear explosions on Amchitka Island. Attempts to simulate the structure lead to models of the type shown in Fig. 1. 1. This structure is about 80 km thick and

Fig. 1.1

Plate structure beneath Amchitka Island (Longshot) in the Central Aleutians. Solid dot is location of the earthquake studied in this report.

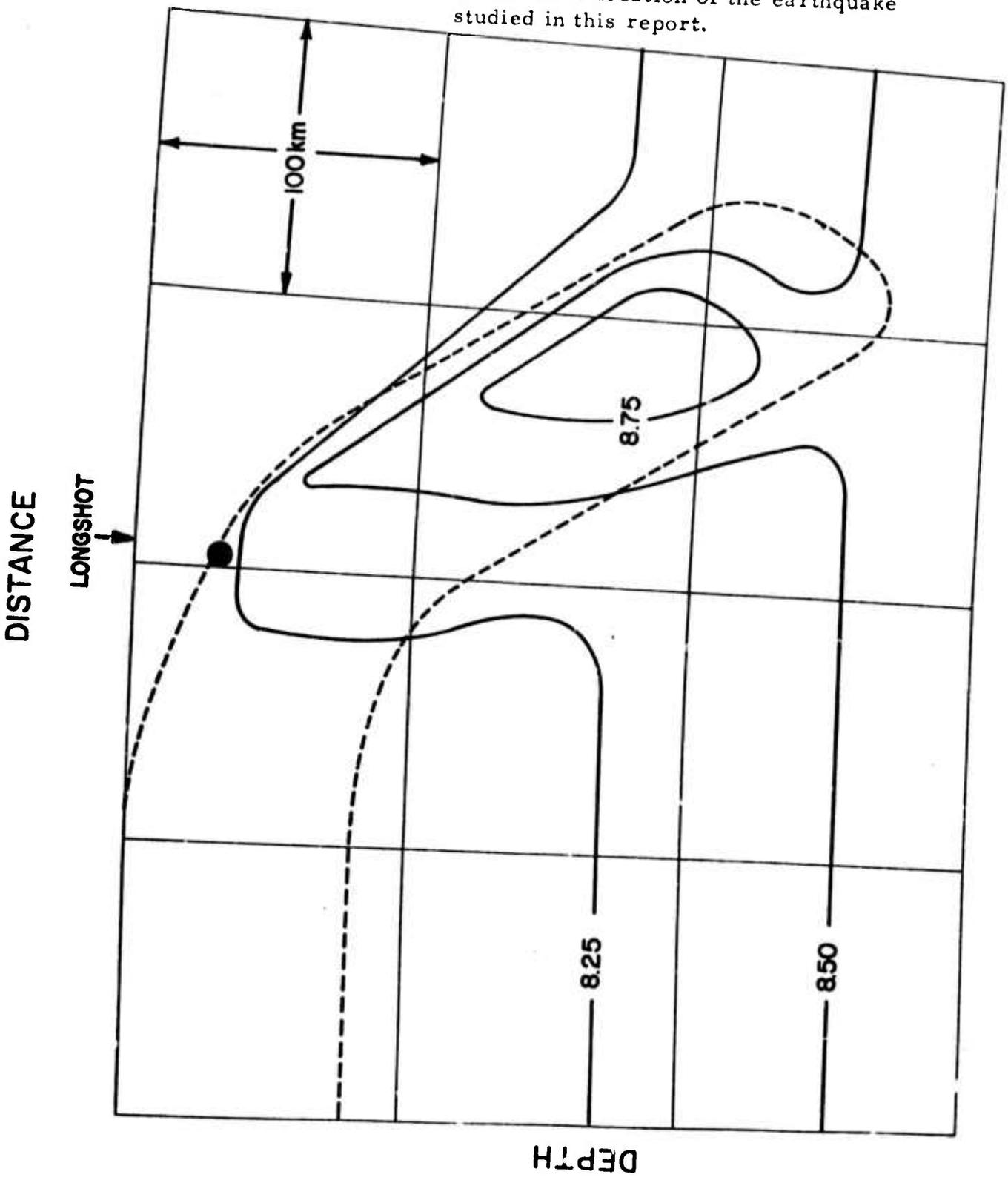

penetrates about 250 km into the mantle with a seismic velocity about 7% higher in the center of the plate than in the average upper mantle (Jacob, 1972). The location of the plate with respect to the Longshot explosion is fixed most accurately from the observed amplitudes of teleseismic P waves (Sleep, 1973). The velocity model shown in Fig. 1.1 was constructed from the 1968 velocities of Herrin et al. and a numerically calculated thermal model of the slab in the manner described by Sleep (1973, equation (1)).

The problem of ray tracing in a generally heterogenous medium has been described by Julian (1970) and by Engdahl (1973). The calculations are considerably simplified by assuming the plate structure described to be symmetric about the center of curvature of the island arc in the vicinity of Amchitka. An iterative procedure is used to converge on source-receiver ray paths.

The event chosen for study occurred near Amchitka Island during the 1965 Rat Islands earthquake sequence and is located with respect to the plate model in Fig. 1.1. A conventional focal mechanism solution, corresponding to overthrusting of the island block relative to the oceanic block has been published by Stauder (1968, event 8, Table 1). The slip vector for this solution (N39W) was used by Minster et al. (1974) to determine the relative plate motion.

The original P- wave first motion data and nodal planes published by Stauder for this event are plotted, using the Herrin 1968 conventional Earth model, on the lower half of the focal sphere in Fig. 1. 2a. The same rays were then traced through the plate structure shown in Fig. 1. 1 and their projections on the focal sphere are shown in Fig. 1.2b. Rays to stations COL and CMC were not traced because their paths would sample considerably more of the Aleutian arc than has been modelled here.

Introduction of plate structure has produced changes in the focal angles from this event of up to 8° in dip and 19° in azimuth to some stations. Ray projections to North America appear to have undergone a net outward shift and counterclockwise rotation, as these rays seek the higher velocity path through the plate. Ordinarily, these changes might not affect the location of the nodal planes, as in the case of intermediate depth earthquakes in the central Aleutians (Engdahl, 1974). In this particular case, however, the strike of the auxiliary plane is highly dependent on stations to North America (NE quadrant). If the fault plane is held fixed, we find a new solution for the auxiliary plane which requires a 2° change in dip and a 12° change in dip direction. The slip vector undergoes a corresponding rotation from N39° W to N51° W.

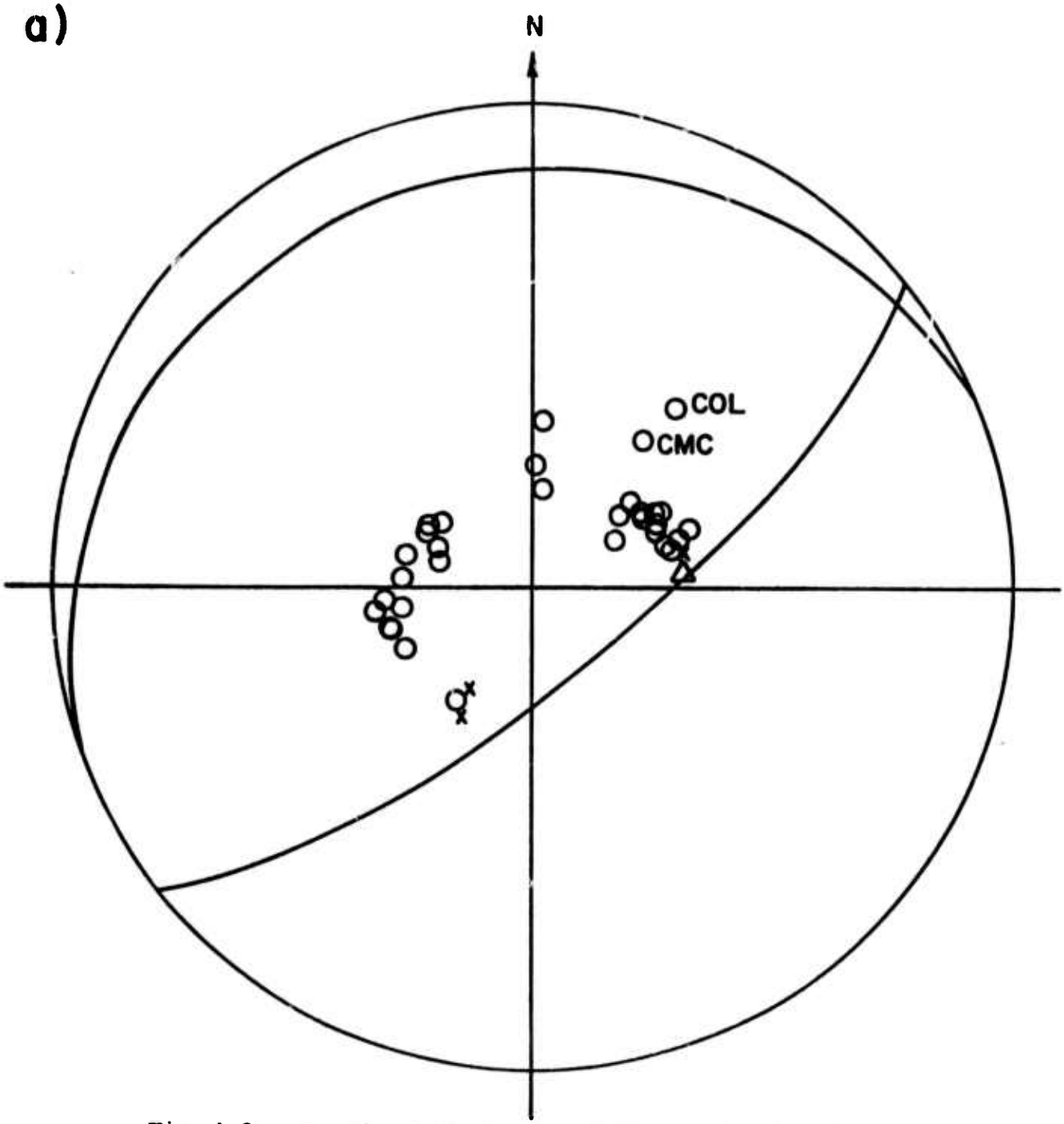


Fig. 1.2a. Focal mechanism (equal area projection) from a conventional Earth model. Circles represent compression P first motions and triangles rarefaction. Crosses represent P-wave arrivals that appear to be near nodal lines.

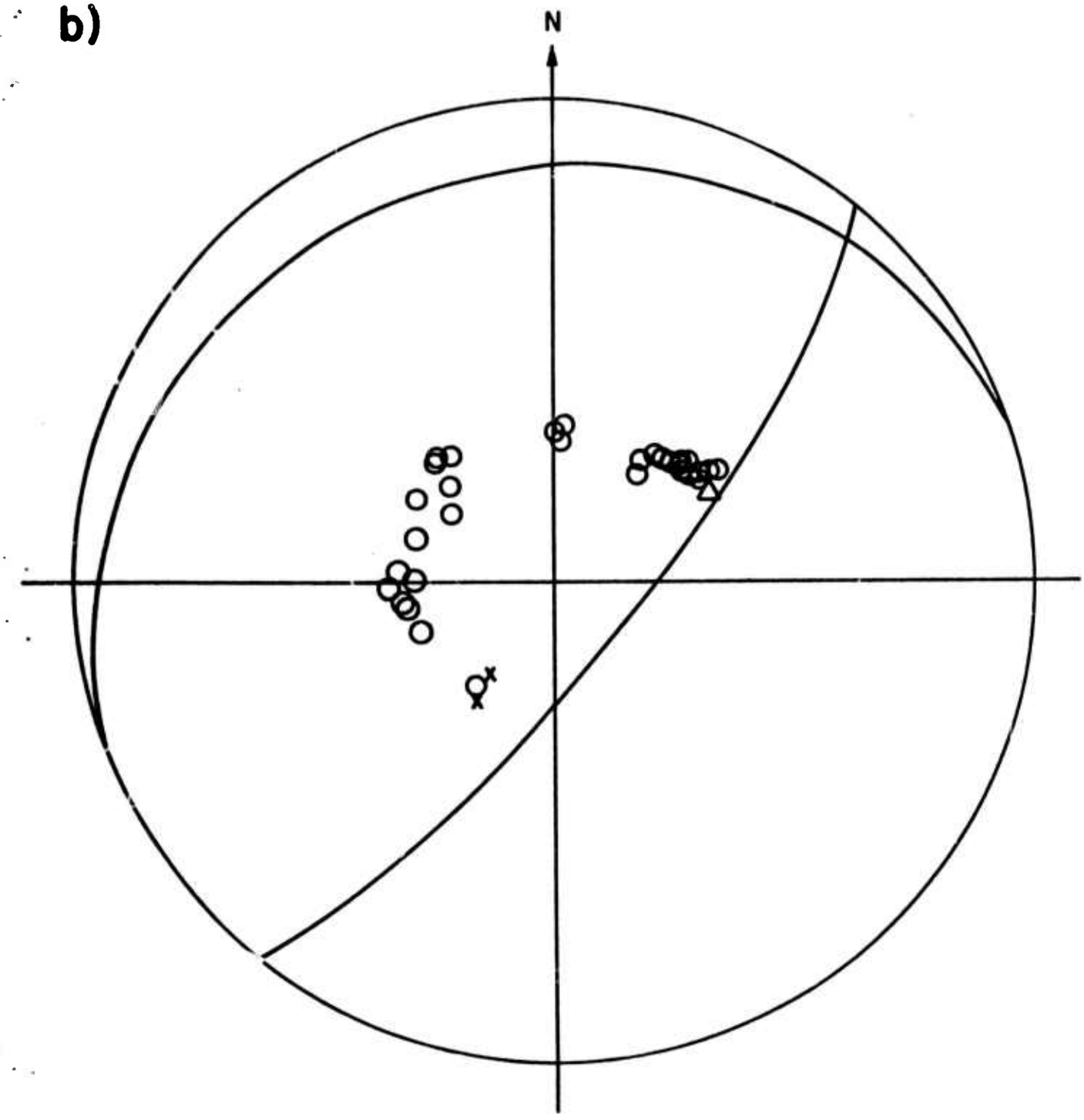


Fig. 1.2b

Focal mechanism from a model incorporating plate structure.

This obvious discrepancy in the slip vector has an important consequence in the modelling of relative plate motions. Because of the similarity in source-station geometry along the whole of the Aleutian arc, we could expect to have the same discrepancy in other solutions published by Stauder. Minster et al. relied heavily on these data to propose the existence of a Bering plate, moving with respect to North America. The Bering plate was introduced because of a systematic misfit to the slip vectors of earthquakes along the Aleutian and Kuril arc for a pole (NOAM-PCFC) determined by assuming the lithosphere north of the Aleutian arc as part of the North American plate. This misfit to the slip vectors is of the same magnitude and direction as the changes in the slip vectors produced by redetermining the focal mechanisms with a plate structure using seismic ray tracing.

In conclusion, plate structure may significantly affect earthquake focal mechanism solutions in active subduction zones. In the particular case of the Aleutian arc errors in the slip vectors of 12° are observed. This result obviates the need for a Bering plate in the modelling of relative plate motions in the North Pacific.

The cooperation of the National Center for Atmospheric Research in permitting the use of their CDC 7600 computer for the purpose of expediting the development of the computational techniques used in this research is gratefully acknowledged.

## References

Davies, O. & Julian, B. R., 1972. A study of short period P-wave signals from Longshot, Geophys. J. R. astr. Soc., 29, 185-202.

Engdahl, E. R., 1973. Relocation of intermediate depth earthquakes in the central Aleutians by seismic ray tracing, Nature, Phys. Sci., 245, 23-25.

Engdahl, E. R., 1974. Effects of island arc plate structure on earthquake hypocenters and focal mechanisms (abstract), Trans. Am. geophys. Un., 55, 348-349.

Herrin, E. (Ed.), Arnold, E. P., Bolt, B. A., Clawson, G. E., Engdahl, E. R., Freedman, H. W., Gordon, D. W., Hales, A. L., Lobdell, J. L., Nuttli, O., Romney, C., Taggart, J. & Tucker, W., 1968. 1968 Seismological Tables for P Phases, Bull. seism. Soc. Am., 58, 1193-1352.

Jacob, K. H., 1972. Global tectonic implications of anomalous seismic P travel times from the nuclear explosion Longshot, J. geophys. Res., 77, 2556-2573.

Julian, B. R., 1970. Ray tracing in arbitrarily heterogeneous media, Lincoln Laboratory Technical Note 1970-45.

Minster, J. B., Jordan, T. H., Molnar, P. & Haines, E., 1974. Numerical modelling of instantaneous plate tectonics, Geophys. J. R. astr. Soc., 36, 541-576.

Sleep, N., 1973. Teleseismic P-wave transmission through slabs, Bull. seism. Soc. Am., 63, 1349-1373.

Stauder, W., 1968. Mechanism of the Rat Island earthquake sequence of February 4, 1965, with relation to island arcs and sea-floor spreading, J. geophys. Res., 73, 3847-3858.

## 2. A P Travel-Time Residual Study of the Hindu Kush Region

E. R. Engdahl

In this study P- time residuals from events occurring in the Hindu Kush seismic zone are systematically evaluated as a means of developing some detailed information on lateral variations in the crust and upper mantle of the region. Preliminary results are presented on a residual-sphere in the manner described by Davies & McKenzie (1969).

The source of data is the ISC Bulletins. All events occurring in the Hindu Kush seismic zone and a small nearby source in India as reported by the ISC for 1964-1970, were sorted by recording station and by source region within the overall zone as described in Table I.

Table I

| Source Region | Latitude (°N) | Longitude (°E) | Depth (km) |
|---|---|---|---|
| Hindu Kush Source | 36-37 | 70-72 | 170-260 |
| Hindu Kush Intermediate | 35-39 | 69-76 | 80-170 |
| Hindu Kush Shallow | 35-38 | 67-75 | 0- 80 |
| Indian Shallow | 29-31 | 67-71 | 0- 80 |

The residuals for each source-station pair were then plotted on film as functions of the number of stations reporting the event, time, latitude, longitude, and depth. These plots were examined for degree of scatter and stability of mean residual at individual stations. At most stations the means were quite stable. No dependence on number of stations or time was observed. However, at close distances, some stations were highly sensitive to position within an individual source region. This effect will be examined more closely at a later date.

The next step was to plot stable mean residuals on the residual-sphere. This was accomplished by using the mean depth and mean azimuth for all events within a particular source-station group to determine the focal angle. Those source-station pairs having a standard error of the mean residual (SEM) less than 0.15 sec. are plotted in Figs. 2.1-2.4 for the four source regions considered. No distinct pattern is recognizable in these initial plots. This is not unexpected since we have not yet removed first order effects of the crust and mantle beneath the recording station. There are two ways to remove the station effect: 1) subtract the residuals from a nearby source likely to have a "normal" mantle beneath it; 2) Subtract station corrections independently derived from deep-focus events (> 300 km) occurring in other regions.

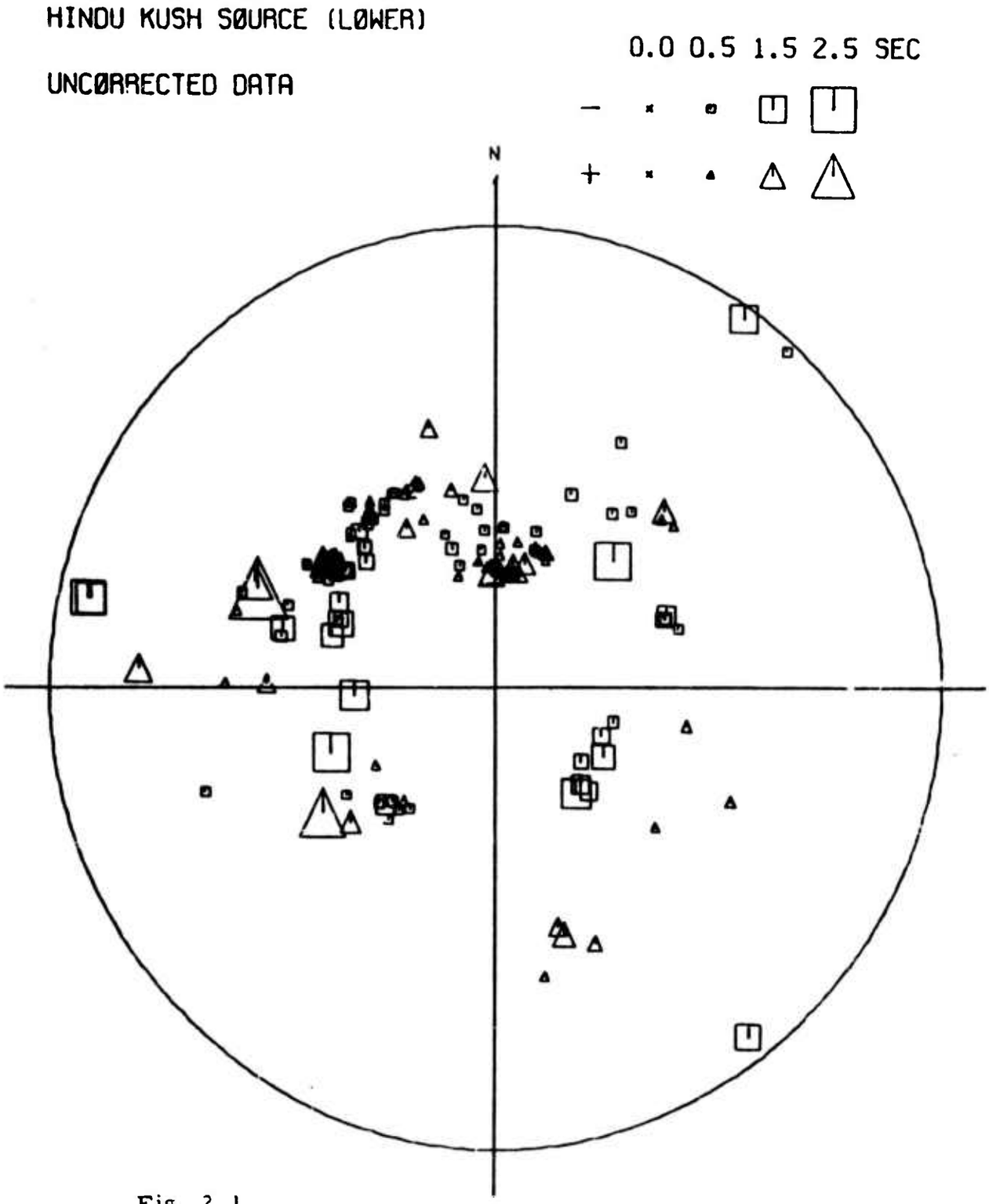


Fig. 2.1

HINDU KUSH INTERMEDIATE (LØWER)

UNCØRRECTED DATA

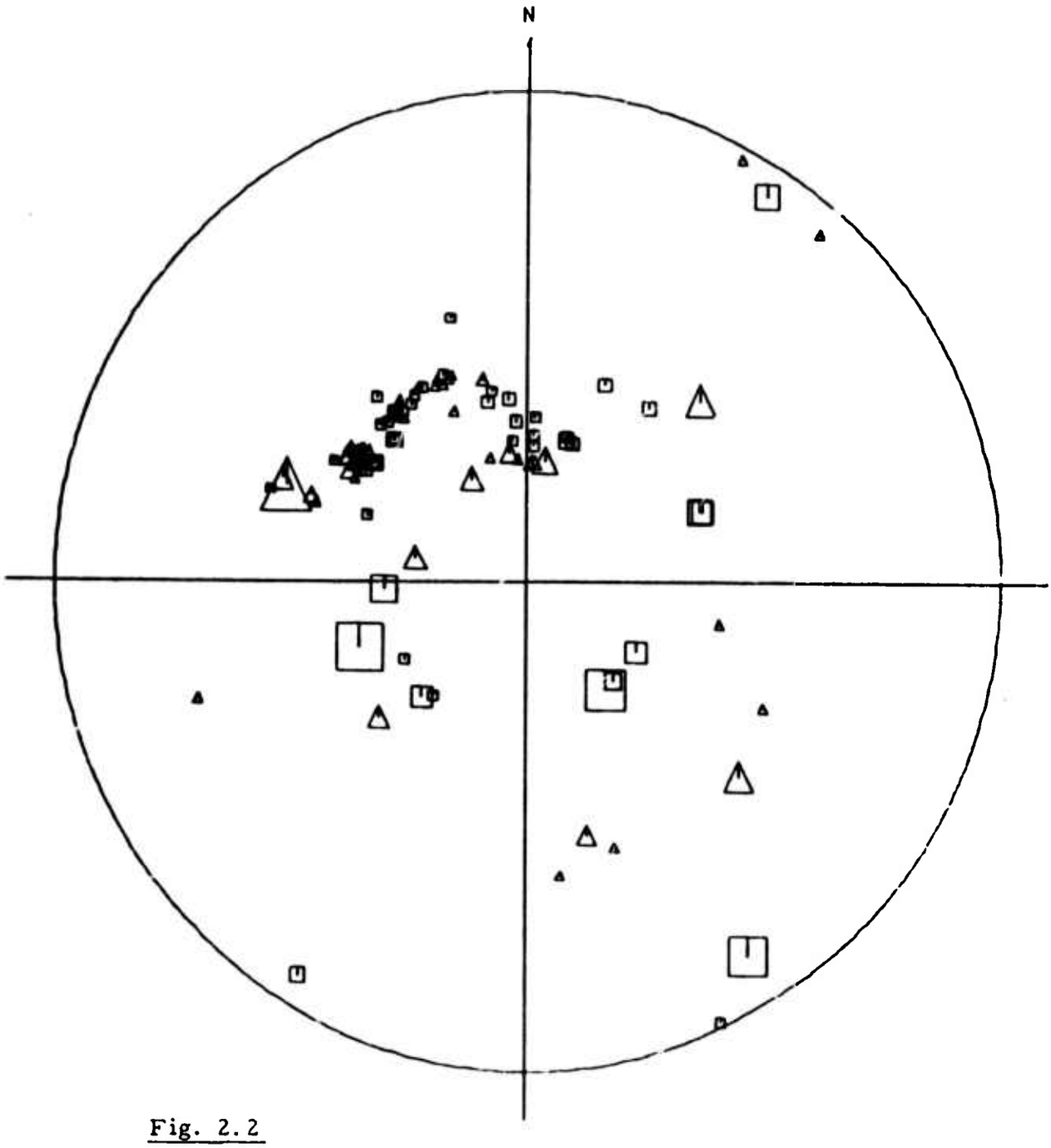


Fig. 2.2

HINDU KUSH SHALLØW SØUTH (LØWER)

UNCØRRECTED DATA

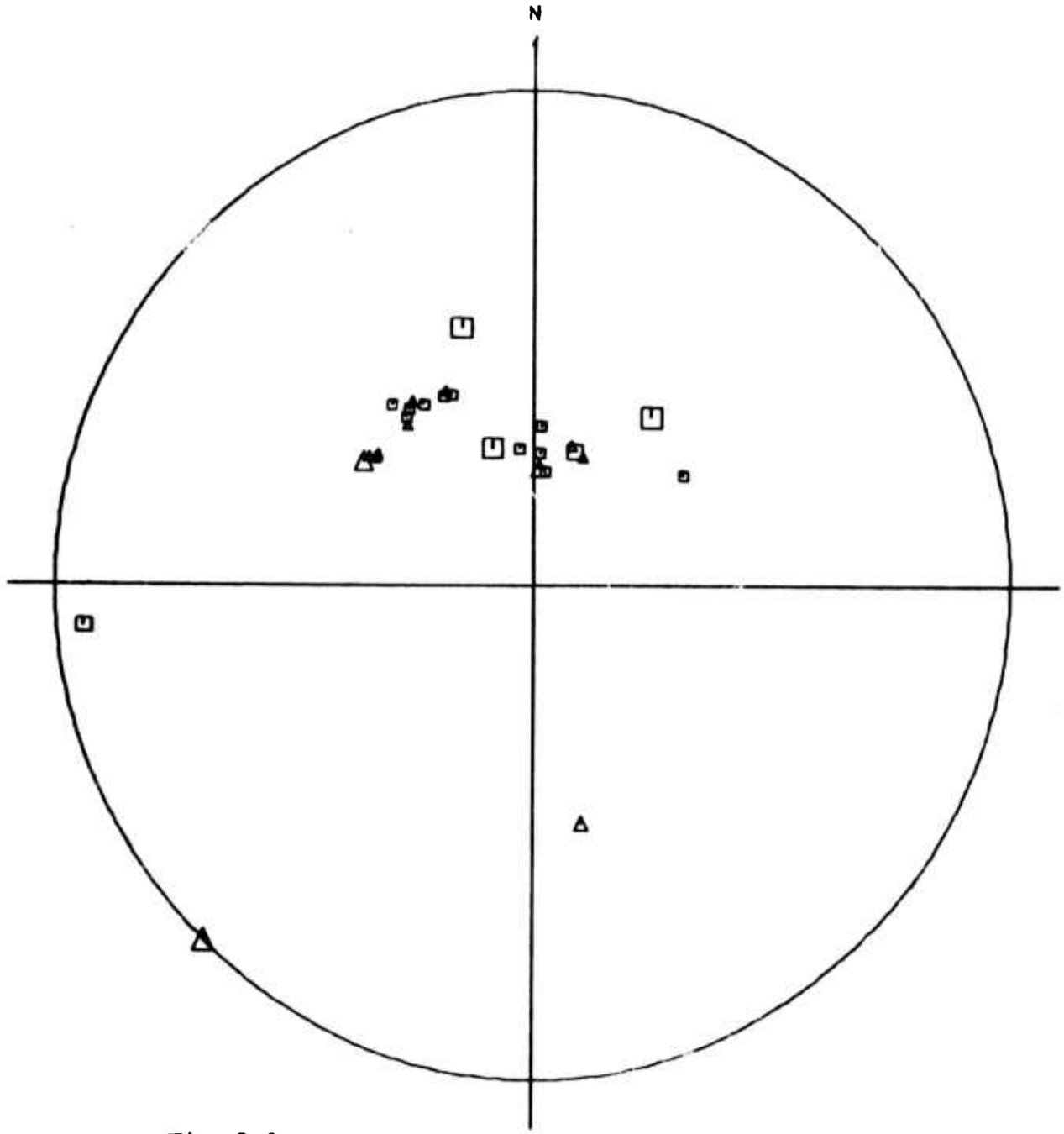


Fig. 2.3

INDIAN SHALLØW (LØWER)

UNCØRRECTED DATA

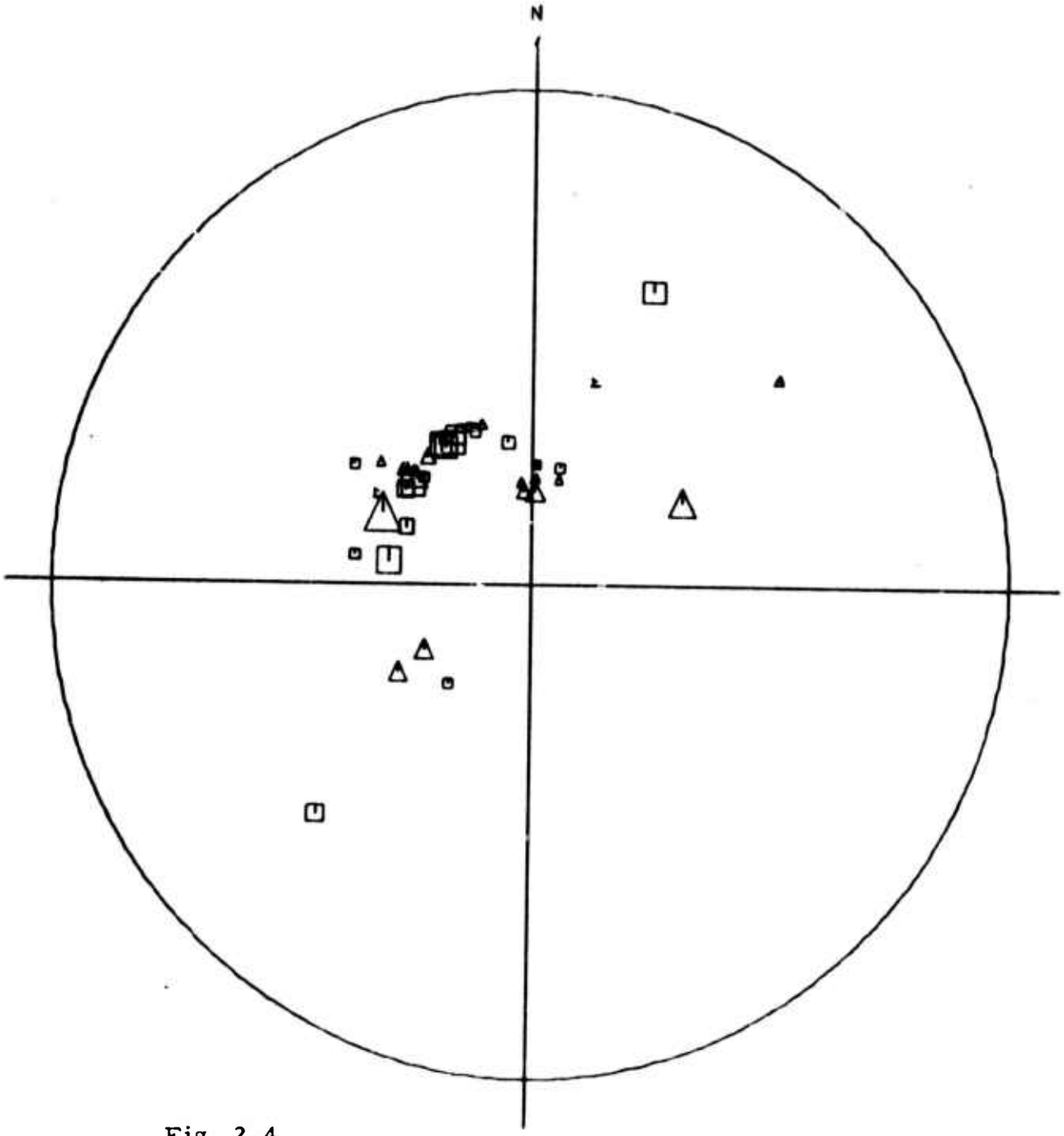


Fig. 2.4

To test the former method we were fortunate to have an active source in the continental Indian plate south of the Hindu Kush. Subtracting residuals for stations common to both sources and meeting our criteria for SEM we obtain the residual-sphere plots shown in Figs. 2.5-2.7. Common to these plots is a central zone of negative residuals and an outer region of positive residuals. One of the properties of the residual-sphere is that it can be treated by fault plane methods. The curve drawn through the "fast" regions of the residual-sphere is an equal area projection of a great circle with a dip of about 12° and a strike of about N35° E, suggesting at least in part a planar mechanism near source for producing the residuals.

Support for these results can be shown using the second method of removing station effects. In Figs. 2.8-2.9 are plotted residuals for Russian stations from which station corrections previously determined (Semi-Annual Report No. 1) were subtracted. The pattern is strikingly similar to that obtained by the source-subtraction method. Station corrections are now being determined for other observing stations and the results will be presented at a later date.

These new data suggest that the Hindu Kush seismic zone lies in a planar zone of high-velocity material, possibly a fossil plate, extending beneath the Hindu Kush source (~ 210 km) and dipping steeply to the northwest.

HINDU KUSH SØURCE (LØWER)

DATA LESS INDIAN SHALLØW

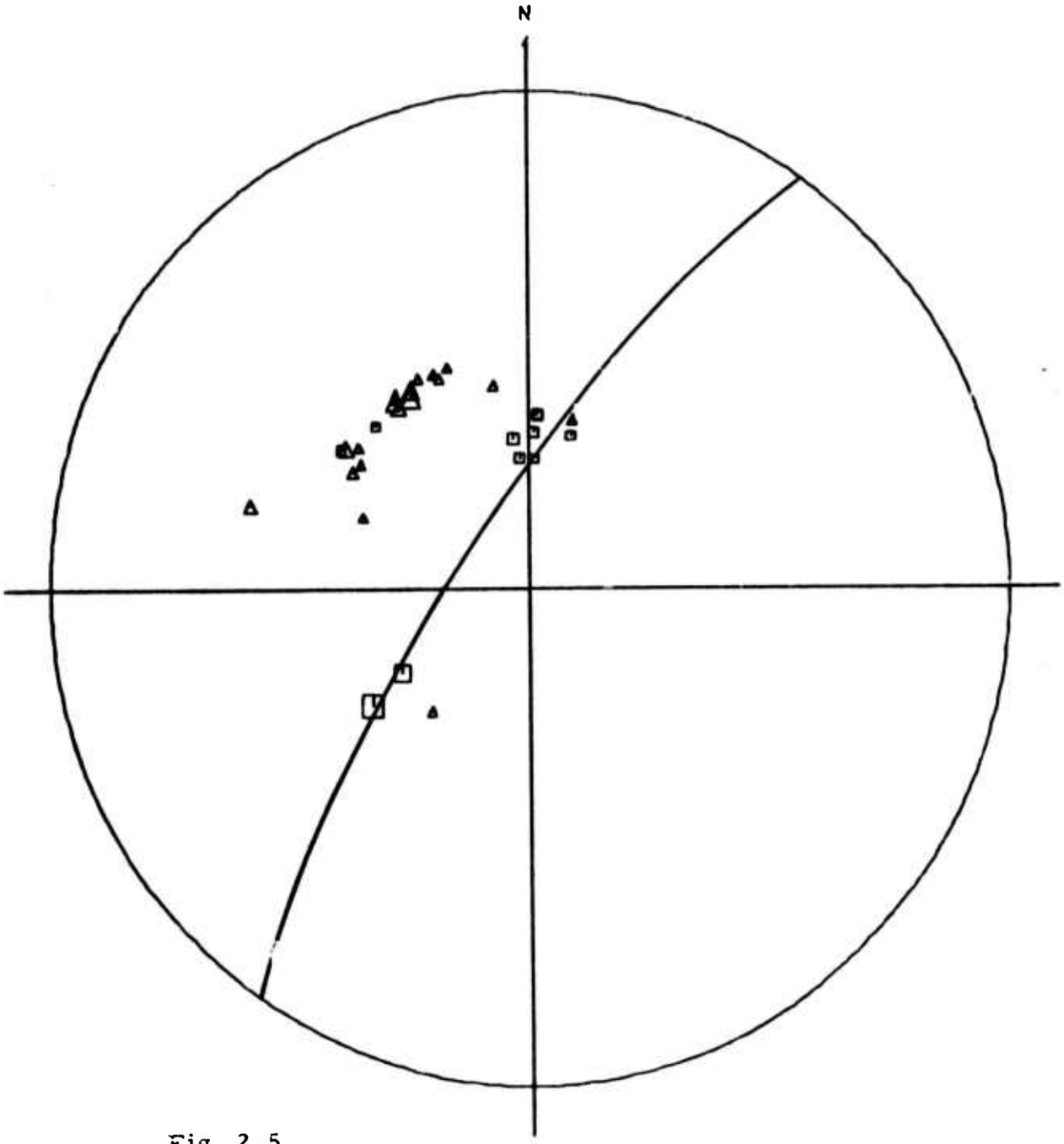


Fig. 2.5

HINDU KUSH INTERMEDIATE (LØWER)

DATA LESS INDIAN SHALLØW

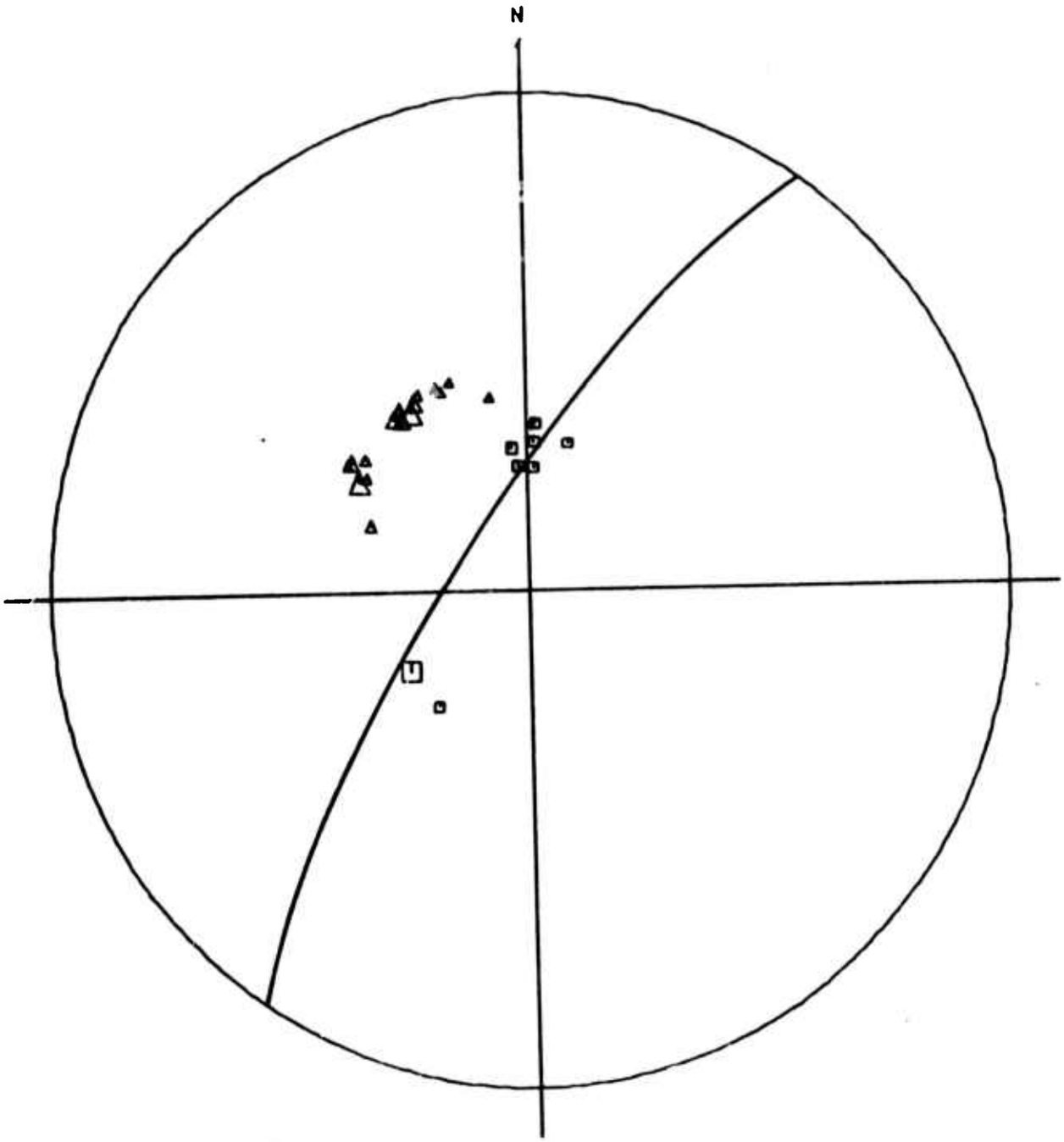


Fig. 2.6

HINDU KUSH SHALLØW SØUTH (LØWER)

DATA LESS INDIAN SHALLØW

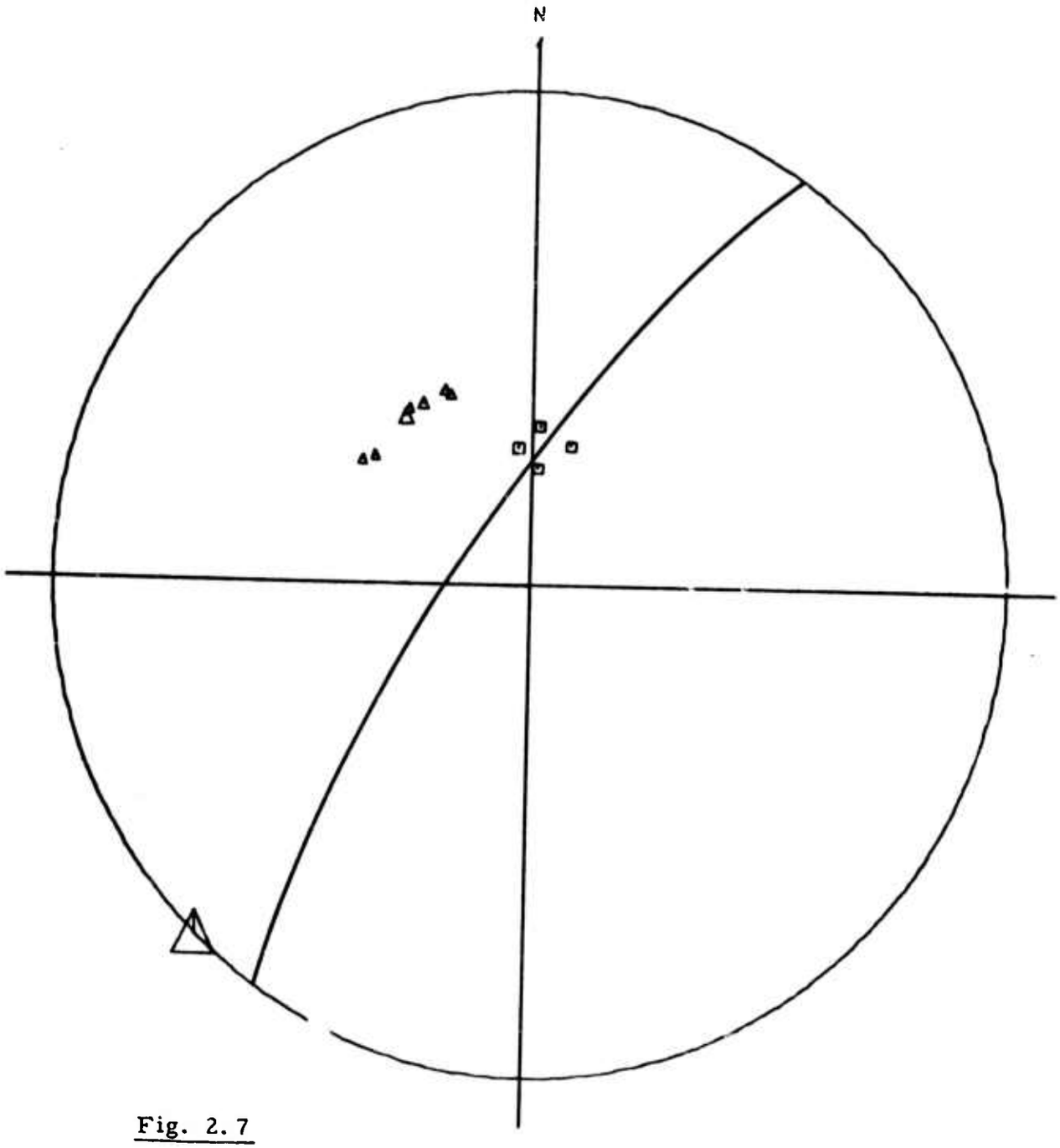


Fig. 2.7

HINDU KUSH SØURCE (LØWER)

DATA STATIØN CØRRECTED

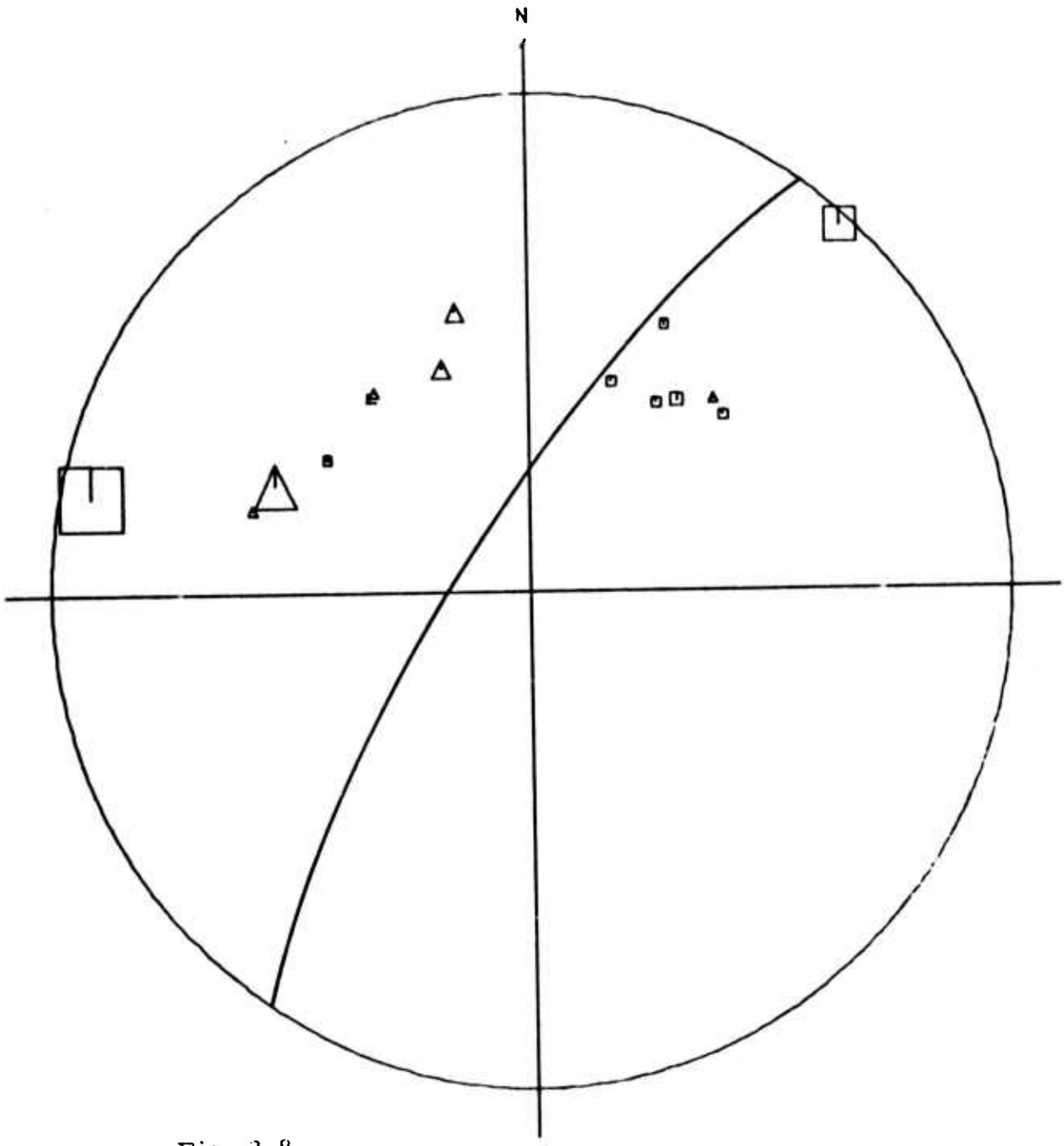


Fig. 2.8

HINDU KUSH INTERMEDIATE (LØWER)

DATA STATIØN CØRRECTED

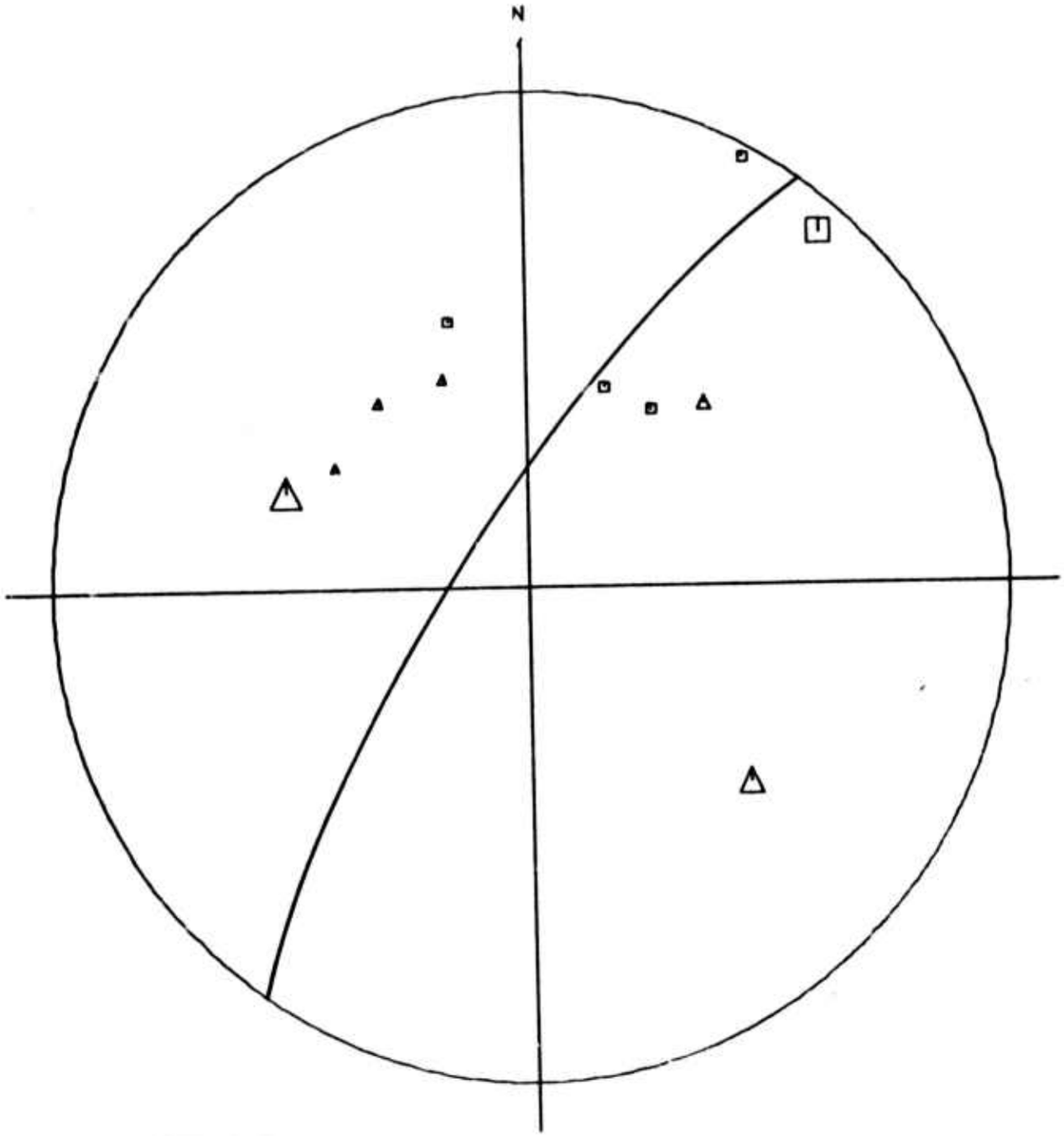


Fig. 2.9

References.

Davies, D. & D. P. McKenzie (1969). Seismic travel-time residuals and plates, Geophys. J. R. Astr. Soc., 18, 51-63.

## 3. Long Period Body Wave Studies of Asian Seismic Events

Gary Boucher

Research in this period has been concentrated upon refinement of the detectability of long-period body waves of earthquakes as small as magnitude $m_b$ 5 and of explosions of magnitude $m_b$ 6 and under. Information derivable from earthquake signals that are below the noise level on raw HGLP digital seismograms included arrival time and frequency content data on long period body waves, particularly S waves. Several lines of evidence useful in discriminating between underground explosions and earthquakes are suggested. The work may be divided into two phases as follows:

a) Improvement of signal-to-noise ratio of seismic body waves as recorded on real seismograms, primarily by multiplication of vertical and radial components of motion, with appropriate phase shifts for various types of waves.

b) Use of long period S-waves to refine the origin times of poorly determined small events. An example is shown of a poorly located earthquake with anomalously small $Ms/m_b$ statistic, which evidently occurred much deeper than the poor quality PDE location indicates, with a correspondingly later origin time.

The philosophy of the rather simple minded approach to signal analysis will be discussed, along with suggestions for future development and application of the techniques.

The starting point for a useful method of signal enhancement to detect the presence of long-period body waves on noisy seismograms rests with the observation by Oliver and Major (1960) that the long period energy associated with body waves is predominantly in the form of so-called 'leaking modes', also called PL modes. These modes, which account for the long-period dispersed wave motion associated with body waves, are characterized by particle motion of the prograde elliptical type, in which the phase of the radial component of ground motion is a quarter wavelength behind that of the vertical motion. Such wave motion was originally discussed in terms of P waves, but was subsequently shown to be associated with vertically polarized S- waves. Since leaking modes by definition are highly attenuated, and since they are in effect continuously generated by incidence of the associated body wave upon the free surface of the earth, the dispersion is controlled primarily by the crustal structure along the propagation path within a relatively small distance of the recording station. Thus there is considerable similarity between PL waves as observed from different events at a given station, as long as the direction of approach and epicentral distance are not too different.

Utilizing the elliptical particle motion as the basis for analysis, it is clear that multiplying together the vertical and radial components of the signal, in the sense of point-by-point multiplication of the values of the time series, especially if the phase of the radial component is increased by a 90°, will yield a rectified, dominantly positive wave form on the product trace. A further advantage is in the reduction of the background noise, since a small amplitude on either trace will yield a small value of the product trace, and since energy lacking the proper phase relationship will appear on the negative side of the product trace. The following examples will show that the technique of multiplying components together is very effective in reducing both background microseisms and the signal-generated noise common to seismograms that generally aggravates the detection of phases arriving after the beginning of the record. In a representative example, where the amplitudes on the original seismogram are large enough to measure, the improvement in signal to noise ratio (as measured from the seismogram with a scale) is at least a factor of 10 referred to the signal-generated noise before a large PS phase, and at least a factor of 20 referred to the microseisms preceding the P-wave arrival. This may be seen from Fig. 3.1 which shows records records from Albuquerque, New Mexico at a distance of 109° from

an earthquake in Northwestern Kashmir. Multiplying of components without phase-shifting the radial component also gives considerable enhancement in signal-to-noise ratio, but perhaps not quite as much as with the phase shift, and this procedure does not give the positive, rectified appearance that is instantly diagnostic of the shifted product of the sought-for wave types. The reduction of noise level seems to be slightly inferior in the multiplication without phase shift. Throughout this work, the instrumental phase shifts have not been explicitly treated, as they are not known at present. The assumption that the phase shifts between instruments are similar appears to be reasonably well justified in most cases, although at very long and very short periods there may be a problem.

The following detailed points about Fig. 3. 1 may be noticed. First, for the PS phase shown, which is large enough that a signal-to noise comparison may be made roughly quantitatively, the improvement in signal to noise, based upon apparent zero to peak amplitudes (that is, measurements made from the seismograms with a scale) is at least a factor of 10 for the product trace, referred to the earthquake-generated signal preceding PS, and at least a factor of 20 referred to the microseism level prevalent before the arrival of the P wave. Since the product records have dimensions of amplitude squared, the numerical value of the improvement

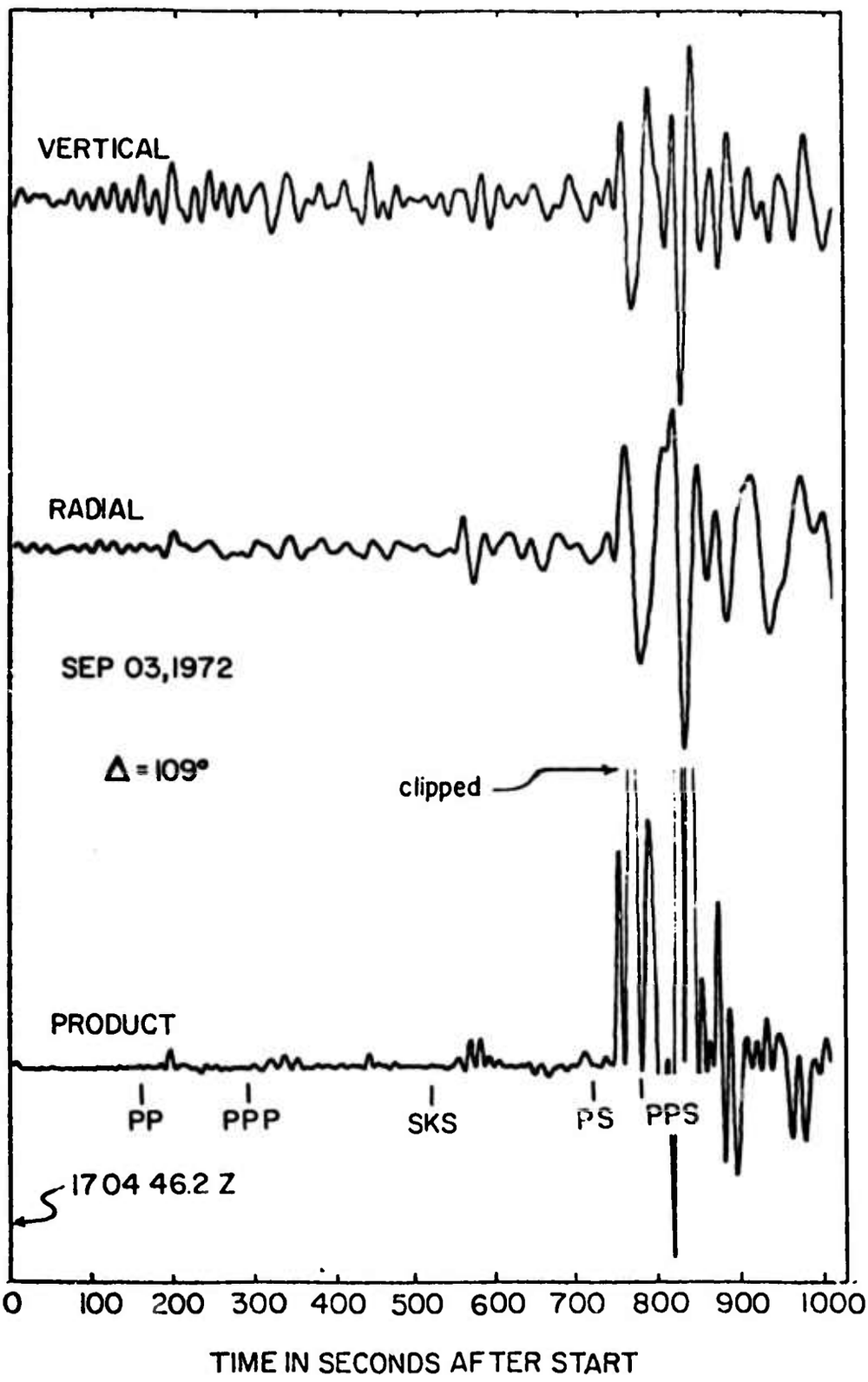
VERTICAL
RADIAL
SEP 03,1972
Δ = 109°
clipped
PRODUCT
PP
PPP
SKS
PS
PPS
1704 46.2 Z
0
100
200
300
400
500
600
700
800
900
1000
TIME IN SECONDS AFTER START

Fig. 3.1

Figure 3.1

Records from Albuquerque, New Mexico HGLP station for the earthquake of Sept. 3, 1972 at 16 42 28.8 Z. (Northwestern Kashmir, $m_b$=6.3, $M_s$=6.2). Epicentral distance 109 degrees. Top to bottom are the raw vertical trace, the radial component (transformed from east-west and north-south components), and the product trace, made by multiplying together the radial and vertical components. The phase of the radial component is shifted forward by 90°, to exploit the prograde elliptical polarization of PL-type ground motion. The raw records were also band pass filtered, using upper and lower corner frequencies of 0.10 and 0.02 Hz, respectively, before multiplication. The purpose of the band pass filter is to remove the large amplitude extremely long period background noise, as well as the microseisms with frequencies greater than 0.1 Hz. The body-wave arrival time serves as a fiduciary mark with respect to which the signal in the product trace may be analysed. Notice that the large amplitudes in the product trace are significantly delayed with respect to the body-wave arrival time. This is partly a result of instrumental phase shift, but principally it is due to the dispersed nature of the PL-type of wave motion. At this distance the P wave is very small. The time reference given on all the figures refers to the time at the left hand margin of the picture, the 'start' of the record shown.

in signal-to-noise ratio would appear to decrease at lower amplitudes. However, the smaller arrivals in Fig. 3.1 demonstrate that the improvement in signal-to-noise ratio for phases like PP is such that the arrival of PP is obvious and easy to pick on the multiplied record, whereas on the vertical channel alone it cannot be identified. The records shown in Fig. 3.1 were made at an epicentral distance of 109°. Naturally at shorter epicentral distances body waves from smaller events are detectable. Fig. 3.2 shows the Kipapa, Hawaii records of the same earthquake at epicentral distance of 104°. The PP and PPP phases are somewhat better developed in this case on the product trace.

Figure 3.3 is intended as a practical example of the usefulness of this approach. The earthquake in the example occurs in the same area as the earthquake shown in Figs. 3.1 and 3.2. Its depth is given by the PDE determination as 55 km. On the shifted product seismogram as described above, however, the wave groups that appear to correspond to the S- and SS- coupled PL phases at Kongsberg, Norway are too early by approximately 20 seconds. The inconsistency is easily explained if the depth of the earthquake were around 400 km. The PDE solution is based upon only 8 stations, and uses only P phases, so that the depth is poorly constrained, and a mis-determination of the depth and

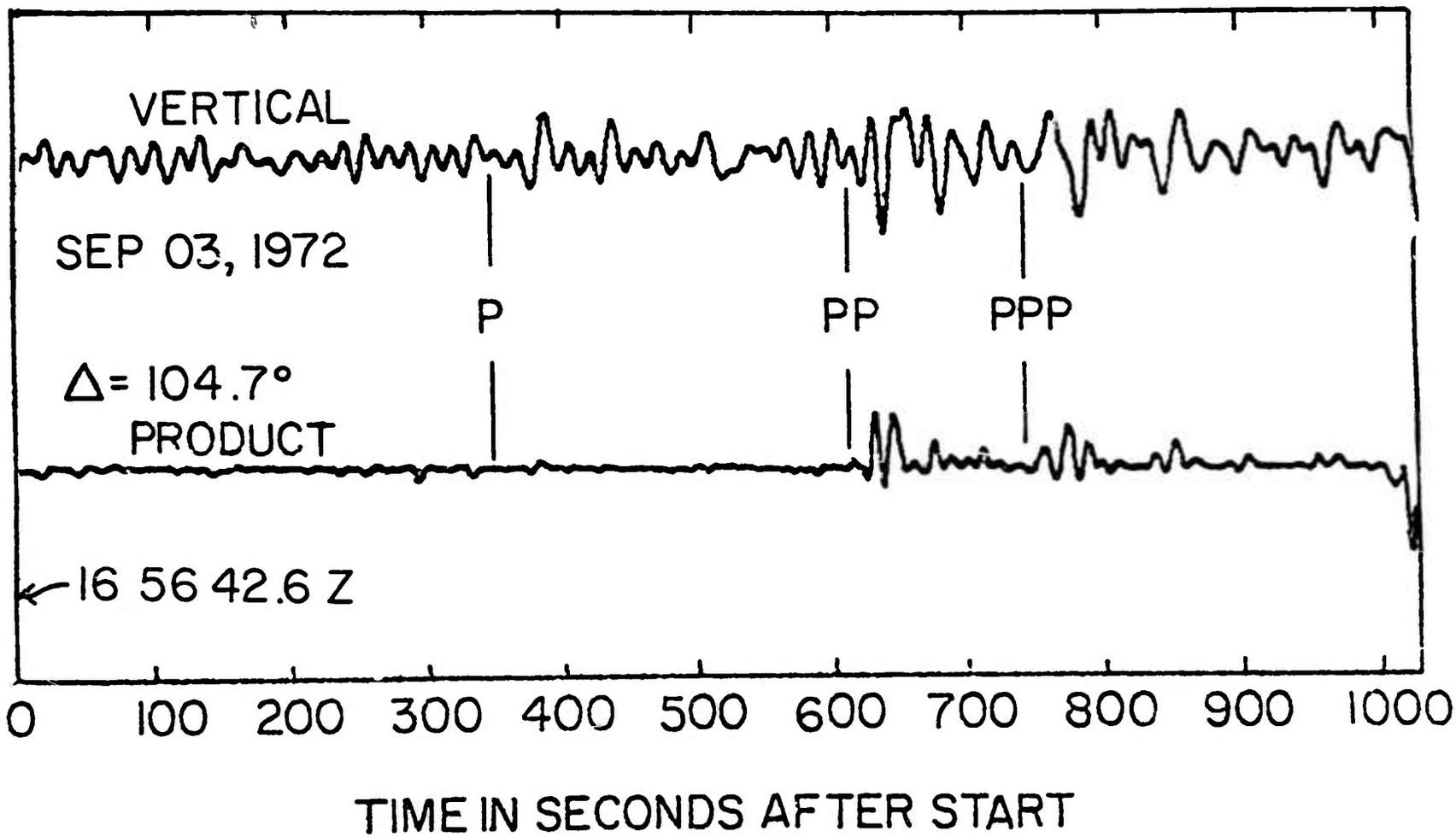


Fig. 3.2. Kipapa, Hawaii, records of the same earthquake as shown in Fig. 3.1. Only the vertical and product traces are shown. In this and the following figures, the radial component is phase-shifted as described in the caption of Fig. 3.1. Again, at this distance the P wave is very small, but PP and PPP can be identified by their prograde elliptical character (which appears as a positive, rectified waveform on the product trace), whereas precise timing of these phases on the raw seismograms is impossible.

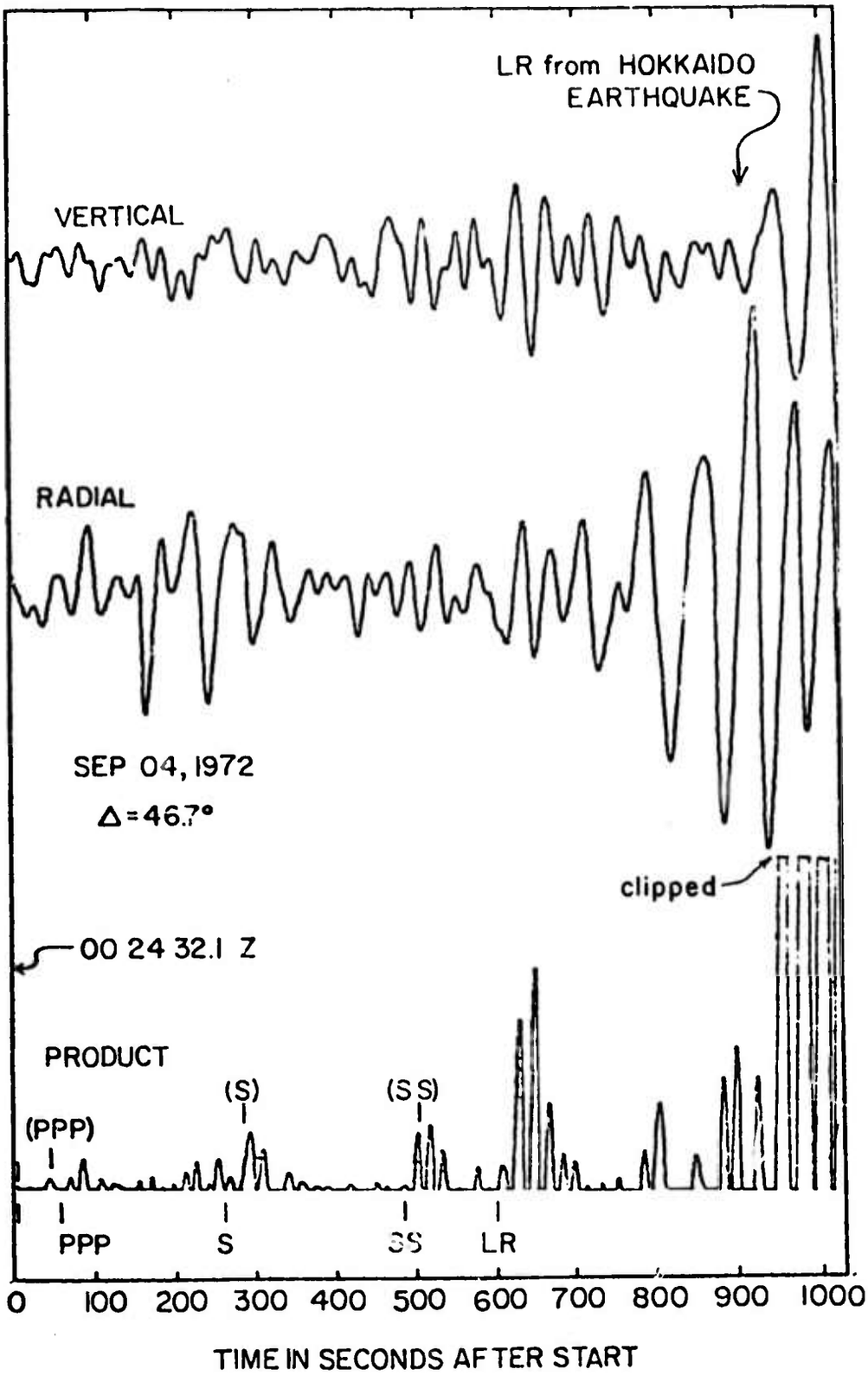
LR from HOKKAIDO
EARTHQUAKE
VERTICAL
RADIAL
SEP 04, 1972
Δ=46.7°
clipped
00 24 32.1 Z
PRODUCT
(PPP)
(S)
(SS)
PPP
S
SS
LR
0
100
200
300
400
500
600
700
800
900
1000
TIME IN SECONDS AFTER START

Fig. 3.3

Figure 3.3

Kongsberg, Norway, records for an earthquake of magnitude 5.5 on Sept. 4, 1972, with epicenter near that of the earthquake shown in figures 3.1 and 3.2. Also present are surface waves from another earthquake of magnitude $m_b$ 5.5 near Hokkaido, about 70 degrees away with a well determined depth of 76 km. The product trace has been half-wave rectified, in effect, by deleting the negative excursions of the trace, to emphasize the PL-type motions for illustrative purposes. Expected arrival times of various body waves are indicated by vertical bars, as labelled. Values parentheses refer to the depth and origin time as reported by the Preliminary determination of epicenters (U.S. Dept. of Commerce). The PL energy clearly arrives too early for these interpretations to be correct. Beneath the product trace are shown predicted arrival times assuming the depth of the event to be 400 km, and the origin time to be about 30 seconds later. These clearly satisfy the data much better, given the constraints on the relationship between product signal arrival time from all other examples studied. As an additional constraint upon the depth of this earthquake, the relative size of surface waves of the Kashmir earthquake and the Hokkaido earthquake of the same $m_b$ but greater distance is indicative of much greater depth for the Kashmir earthquake. The relative surface wave amplitudes are confirmed by other stations.

origin time is easily possible. The results of the long-period body wave analysis from only a single station provide rather convincing evidence that the origin time should be about 40 seconds later than that given, concomitant with the greater depth. The pP phase is not very helpful in this case, since it nearly coincides in time at near stations with the time of PP, if it can be read at all. Another point of evidence in favor of considerable depth for the event is provided by the size of the surface waves. Coincidentally, there is on the same seismogram the surface wave train from an event near Hokkaido, about 70 degrees distant, and having the same magnitude $m_b$. It is obvious that the surface waves are much larger from that event, indicating that it is shallower, and its depth of 76 km is much better determined, since 43 stations were used in the determination. This is a prime example of the important case where an event with an anomalously small $M_s/m_b$ discriminant, with poorly determined depth could be mistaken for an explosion. Conversely, an explosion could be mistaken for a deep earthquake with a poorly determined origin time, and analysis of the S-waves would be instrumental in classifying the hypothetical event as an explosion. With the limited data available in this case, it is fortunate that the large event which occurred in the same area on the previous day is available to aid in the interpretation of the product seismogram,

since the action of phase shifting and multiplying seismograms introduces considerable distortion in the wave forms. The Kongsberg records for the larger nearby earthquake are shown in Fig. 3.4 for comparison.

The last event in this series is a presumed explosion in Eastern Kazakhstan of magnitude $m_b$ 6.2 (Fig. 3.5). Since this event is evidently an explosion, its long period body waves are much smaller than would be expected for an earthquake of the same $m_b$. This alone is diagnostic of the explosion character of the event, but some further information can be gleaned from the records, using the dispersed character of the leaking mode waves associated with S phases. By simply attempting to match the wave forms between this event as an earthquake, using the expected body-wave arrival time as the time reference, it can be seen that there is a definite absence of the very long period energy in the beginning of the wave group, yet later on, when the shorter periods arrive, the correlation with the earthquake signal is good. As an aid in the interpretation, the earthquake seismogram used for comparison could be high-pass filtered, with the corner around 0.1 Hz, before performing the multiplication, to provide a very comparable waveform. Perhaps it would be useful to repeat here an observation from the previous report, which is that the character of PL waves is determined

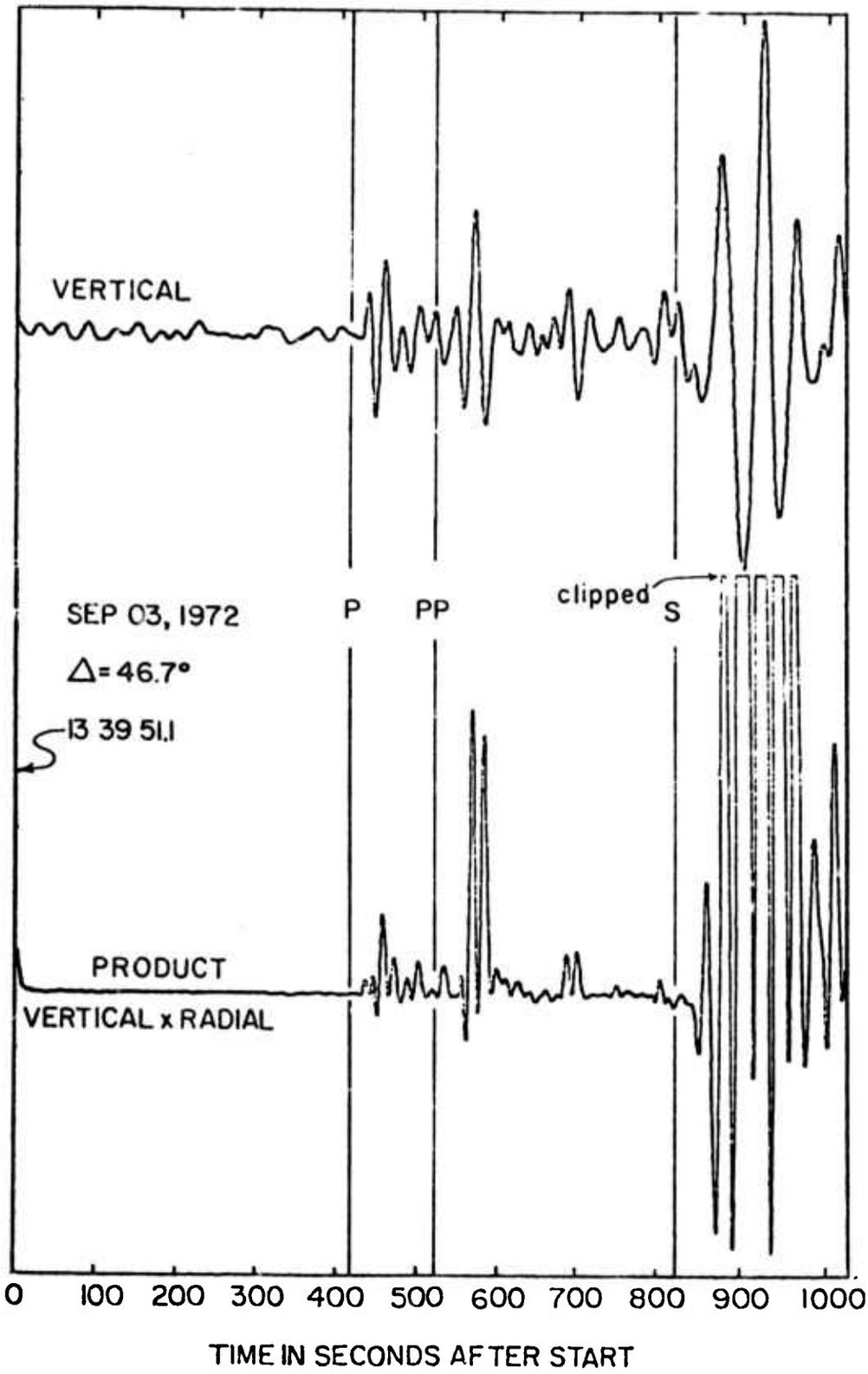
VERTICAL
SEP 03, 1972
Δ= 46.7°
13 39 51.1
P
PP
clipped
S
PRODUCT
VERTICAL x RADIAL
0
100
200
300
400
500
600
700
800
900
1000
TIME IN SECONDS AFTER START

Fig. 3.4

Figure 3.4

Seismograms from Kongsberg, Norway for the Northwestern Kashmir earthquake of Sept. 3, 1972, $m_b$=6.2, depth =36 km, o.t. 16 48 28.8 Z. Depth and origin time for this earthquake are probably well determined. Purpose of this figure, on which the body wave arrival times are well determined, on the raw vertical component, is to show the relationship between predicted body wave arrival time and the arrival of significant amplitudes on the product trace, as developed from the PL-type wave motion. This figure is primarily for reference to Fig. 3.3. and demonstrates that the interpretations of the true body wave arrivals of that earthquake at Kongsberg are reasonable, and that the chosen depth of 400 km represents a lower limit of the acceptable depth for the smaller earthquake in the same region on Sept. 4, 1972.

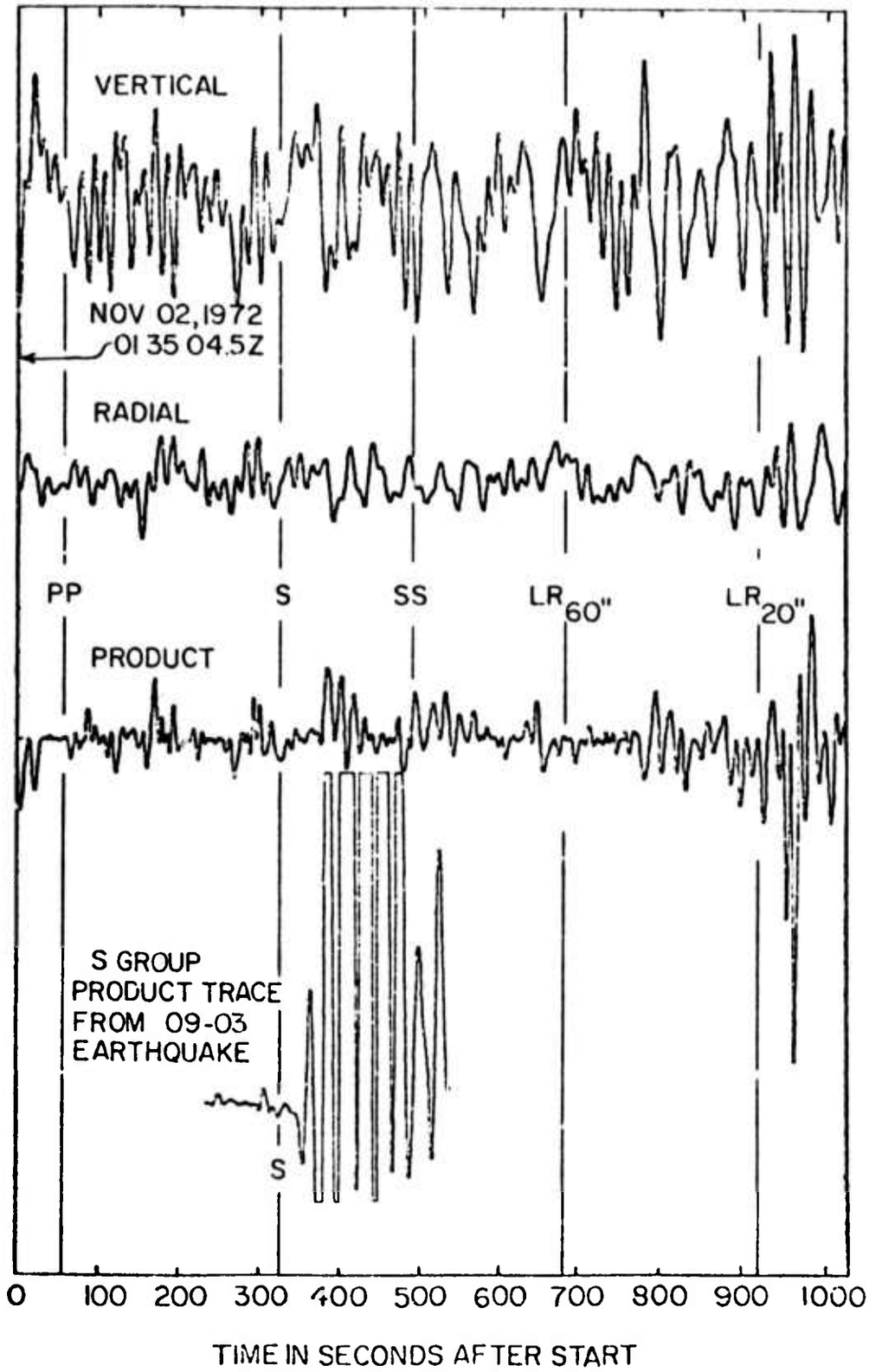
VERTICAL
NOV 02,1972
01 35 04.5Z
RADIAL
PP
S
SS
LR60"
LR20"
PRODUCT
S GROUP
PRODUCT TRACE
FROM 09-03
EARTHQUAKE
S
0
100
200
300
400
500
600
700
800
900
1000
TIME IN SECONDS AFTER START

Fig. 3.5

Figure 3.5

Vertical, radial, and product seismograms from a presumed explosion in Eastern Kazakhstan on Nov. 2, 1972 (origin time 01 26 57.6Z, $m_b$=6.2, PDE). Purpose of this figure is to demonstrate detection of the S phase from the explosion, using the product trace. Included for reference is the S- related portion of the product trace from the Kashmir earthquake of Sept. 3, 1972. It has been observed that the S-waves at a particular station, as seen in the product trace, are generally similar from one event to another, if the direction of approach of the waves is not too different. The close conformity of these two traces, except for scale, of course, in the early high-amplitude portion of the signal, indicates that the assigned depth of the event (namely 0 km) is reasonable. The product races are aligned on the basis of expected arrival time of the S body wave.

largely by the crustal structure within a short distance of the recording station, meaning that the waveforms from different events are quite similar even though the epicentral distances may be significantly different, granting only that the direction of approach of the waves is not too different.

Why this method of analysis?

Some commentary on the philosophy of this type of analysis is in order at this point. The approach used in multiplying records is rather a crude one, and it may seem to be a roundabout way of obtaining spectral and arrival-time information. In fact this approach is dictated by the desire to study events at the lower limit of detectability by single long period instruments. In any given length of record, as may be seen from the original seismograms of either the events in Fig. 3.2 or Fig. 3.4, the spectral density of background noise energy at all frequencies is at least equal to the spectral density of the body wave energy. Therefore computing the Fourier spectrum of a section of record will be of dubious value by itself. The noise must be dealt with in some fashion, since it cannot be removed explicitly. Use of more than one component of motion, exploiting the known polarization of the signals associated with body waves is therefore dictated. It is likely that cross spectral analysis of the radial and vertical

components of motion, exploiting the expected phase characteristics of the signals would accomplish much the same ends.

The advantages of the present method lie in its simplicity, in the real advantage of the non-linearity of the method, and in the fact that the dispersion although equivalent to the phase relationships, is easier to interpret from the product seismograms than from the phase spectra. The aspect of simplicity primarily means a saving in computer time. As is generally true in seismology, the smaller events are more numerous than the larger ones in any given class, and this evidently applies to nuclear explosions as well as to earthquakes, although for different reasons. Thus if small events are of concern, one must be prepared to deal with large numbers of events, and economy of operations is a virtue. The non-linearity, although it takes one a step further from reality, has the advantage that those small components of the noise which do not possess the desired phase relationships are made relatively even smaller, since they enter as the squares of small quantities. Use of the time series is preferred in these circumstances mainly because the implicit phase relationships are easy to ascertain visually: the product seismograms can simply be 'read' like other seismograms. Characteristic signal shapes are rather consistent from one event to another at a given station, and timing, as well as a rough estimate of relative frequency content is easy to determine.

Additional comments.

Optimization of data. The HGLP instruments generally record very long period microseisms which completely swamp the very long period energy of small earthquakes. For this reason it has been found useful to perform a high-pass filtering operation on all the data before doing the multiplication of components, using a filter corner frequency of about 0.02 Hz. On the ordinary records, this filtering operation does not significantly decrease the quality of body wave arrivals, whereas it is of great benefit in removing the very long period sinusoidal waves which are of noise origin and serve only to confuse the interpretation of the records. Naturally the removal of this very long period noise is of considerable value when the multiplication operation is performed. Normally when dealing with earthquake signals it is also helpful to filter out some of the highest frequencies recorded, since they are not normally signal-related, and since this removes occasional small glitches from the record. Explosions evidently do contribute energy even in the upper frequency ranges approaching 1 Hz, so that it is perhaps better not to remove the highest frequencies before processing.

S waves. It is very common for the long period S-waves from an event to be larger than the long period P- waves.

This applies to explosions as well as to earthquakes, as explained in the previous semi-annual report. Therefore, in attempting to interpret seismograms of smallest possible size, it may be worthwhile to concentrate upon the S- waves, as long period P- waves may not be detectable, particularly in the case of explosions.

Extension to smaller events. There is room for improvement in the sophistication of the filtering processes used to detect extremely small body waves True SV- wave polarization filters, relying upon a point by point check of the proper phase characteristics between vertical and radial components of motion would be more effective, although more expensive, than the blanket phase shifting technique used here. Likewise use of multiple stations as an extended array might increase the detectability of very small body waves, although this probably would require a substantially increased number of stations to be really effective.

Conclusion.

A genuinely effective, yet simple method of signal enhancement has been described for detection of long-period body wave-associated energy on seismograms of earthquakes of moderate magnitude at large epicentral distances. The use of long-period S- waves detected in the manner described is useful

in the establishment of focal depth of earthquakes, and the long-period S- waves which have been shown in this and previous work to be associated with presumed explosions are likewise useful, in that they can be used to eliminate the hypothesis that a given event might be a deep earthquake instead of an explosion. The lower limit of applicability of these techniques is not yet known, but it is, using body wave magnitudes $m_b$ as the parameter, probably as low as $m_b$=5 for earthquakes and less than $m_b$=6 for explosions. Some improvement, using more sophisticated analysis is very likely possible.

## 4. Classification of Asian Earthquakes

R. Ganse and G. Lundquist

In recent years, Fourier Transforms have been applied to seismograms, and the resulting spectra have been interpreted in terms of earthquake source parameters. In particular, spectral scaling laws have been derived to relate the various magnitude schemes, based on the fact that each magnitude is just a sample, over a small frequency range, of a properly corrected spectrum. Unfortunately, it is readily apparent that all spectral properties of earthquakes can not be described by a single scaling law. The purpose of this study is to determine whether different spectral classes of earthquakes occur within individual seismic zones of Asia, and to determine whether the spectral properties of those earthquakes might be represented by some limited number of individual scaling laws.

Selection of Events.

Four small areas of the Asian continent were selected for study on the basis of apparent number of events. These areas will have been expanded to include all of the following geologic provinces: (1) The Tien Shan Fold Belt (40-45 N, 70-90 E); (2) a section of the high Tibetan Plateau (29-35N, 91-96E ); (3) the block faulted Tsaidam

Basin (36-39N, 90-99E), and (4) the Lake Baikal region (50-57N, 104-113E). Lake Baikal and the western half of the Tien Shan region are in Russia. The other areas are in China. A simple map of the areas is shown in Fig. 4.1.

A list of known crustal events was obtained from the Hypocenter Data File, and events were selected for detailed study which were represented by useable seismograms. The basic data for the first year's work were seismograms from WWSSN and the Canadian Network. Data has been requested from Russia, and a small amount has been received. Russian seismograms should be an important part of the next year's work. A list of events is given in Table I.

Processing.

The seismograms for each event were read for first motion and earthquake magnitude. During this reading from microfilm chips, stations were chosen for digitization on the basis of signal-to noise ratio, distance and azimuth. Distances were restricted to the range 35-80 degrees as much as possible, and a balanced azimuthal distribution was sought.

Seismogram lengths of roughly 70 sec (short period) and 120 sec (long period) were digitized. P- wave data was collected from short-and long-period vertical seismograms.

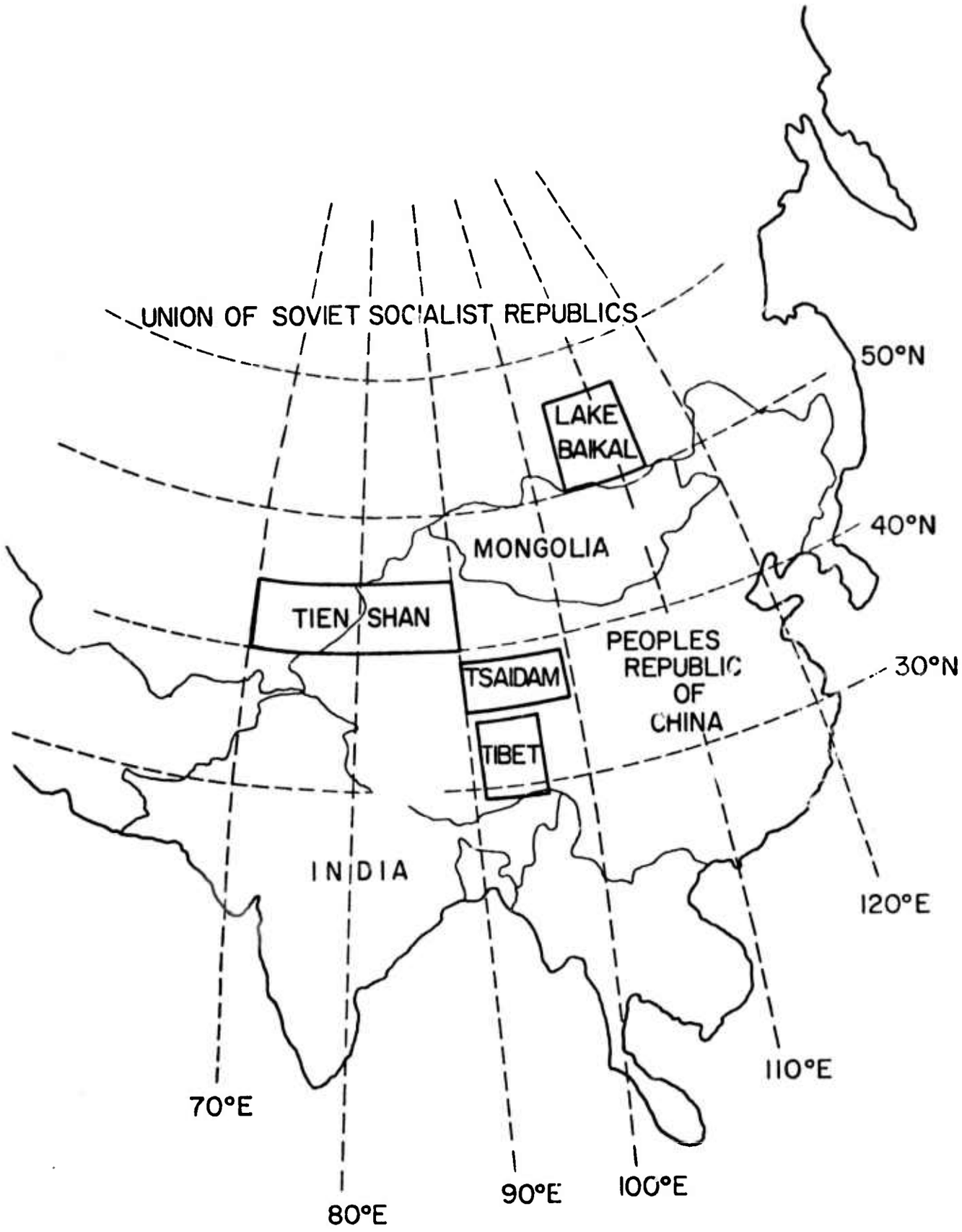


Fig. 4.1

Location map of the regions studied

## TABLE I

| Region | Date | | | Time | | | Location | | Depth |
|---|---|---|---|---|---|---|---|---|---|
| | D | M | Y | H | M | S | N LAT | E LON | (km) |
| Tien Shan | 04 | 05 | 65 | 18 | 34 | 39.8 | 41.71 | 79.4 | 6 |
| | 11 | 02 | 69 | 22 | 08 | 54.7 | 41.35 | 79.21 | 33 |
| | 05 | 06 | 70 | 04 | 53 | 06.4 | 42.48 | 78.76 | 20 |
| | 23 | 03 | 71 | 09 | 52 | 12.3 | 41.49 | 79.26 | 33 |
| | 23 | 03 | 71 | 20 | 47 | 17.4 | 41.45 | 79.26 | 33 |
| | 09 | 04 | 72 | 04 | 10 | 50.7 | 42.18 | 84.65 | 33 |
| | 02 | 06 | 73 | 23 | 57 | 04.2 | 44.10 | 83.55 | 26 |
| Tibet | 15 | 06 | 65 | 07 | 59 | 19.4 | 26.6 | 95.6 | 30 |
| | 01 | 08 | 65 | 14 | 14 | 01.8 | 32.6 | 93.6 | 33 |
| | 15 | 08 | 67 | 09 | 21 | 02.3 | 31.1 | 93.7 | 33 |
| | 14 | 06 | 69 | 03 | 28 | 29.6 | 31.70 | 94.65 | 33 |
| | 03 | 04 | 71 | 04 | 49 | 03.4 | 32.26 | 95.06 | 33 |
| | 22 | 05 | 71 | 20 | 03 | 32.4 | 32.34 | 92.12 | 33 |
| | 22 | 07 | 72 | 16 | 41 | 04.0 | 31.43 | 91.49 | 33 |
| Tsaidam | 21 | 05 | 62 | 12 | 02 | 50.6 | 37.3 | 96.0 | 25 |
| | 19 | 04 | 63 | 07 | 35 | 22.7 | 35.7 | 96.9 | 33 |
| | 01 | 07 | 63 | 21 | 10 | 28.5 | 37.0 | 96.1 | 33 |
| | 16 | 03 | 64 | 01 | 05 | 17.6 | 36.9 | 95.5 | 33 |
| | 14 | 12 | 67 | 19 | 15 | 20.5 | 38.2 | 91 3 | 33 |
| | 24 | 03 | 71 | 13 | 54 | 17.7 | 35.46 | 98.17 | 13 |
| | 30 | 08 | 72 | 15 | 14 | 09.9 | 36.72 | 96.47 | 33 |
| | 30 | 08 | 72 | 18 | 47 | 42.6 | 36.60 | 96.42 | 33 |
| | 16 | 06 | 73 | 07 | 22 | 48.1 | 37.71 | 95.64 | 33 |
| Lake Baikal | 15 | 01 | 67 | 19 | 58 | 42.5 | 55.68 | 110.80 | 11 |
| | 11 | 02 | 67 | 09 | 27 | 30.4 | 52.21 | 106.43 | 5 |
| | 26 | 11 | 68 | 18 | 31 | 51.8 | 55.87 | 111.38 | 4 |
| | 28 | 03 | 70 | 09 | 44 | 57.8 | 52.23 | 105.80 | 33 |
| | 13 | 08 | 70 | 19 | 26 | 55.5 | 51.82 | 105.49 | 33 |
| | 09 | 08 | 72 | 19 | 42 | 17.3 | 52.96 | 107.54 | 33 |

S- wave data was restricted to the short-and long-period horizontal transverse component obtained by a coordinate rotation of the combined NS and EW seismograms. Horizontal particle motion was plotted and the S- wave polarization angle was read, when possible, to be incorporated in focal mechanism determinations.

The digitized seismograms were processed through a Fast Fourier Transform program, and the raw spectra were corrected for instrument response to get station spectra. The processing that led to the meaned "quazi-source" spectra is best described by the flow diagram shown in Figure 4.2. Since the object of this study was not to improve methods for correcting spectra, a minimum of adjustments have been made, and those corrections have used the authors' choice of standard models. The spectra have all been obtained in a consistent manner, and comparison between spectra should depend little on the correction methods used. Figs. 4.3-4.12 show the meaned spectra computed during the first year of this study.

The anelastic attenuation corrections are the only frequency dependent corrections applied to the station spectra. The correction according to CIT 208 is applied to individual stations, and the resulting spectra are those the model would predict if there was no anelastic attenuation in the earth. The

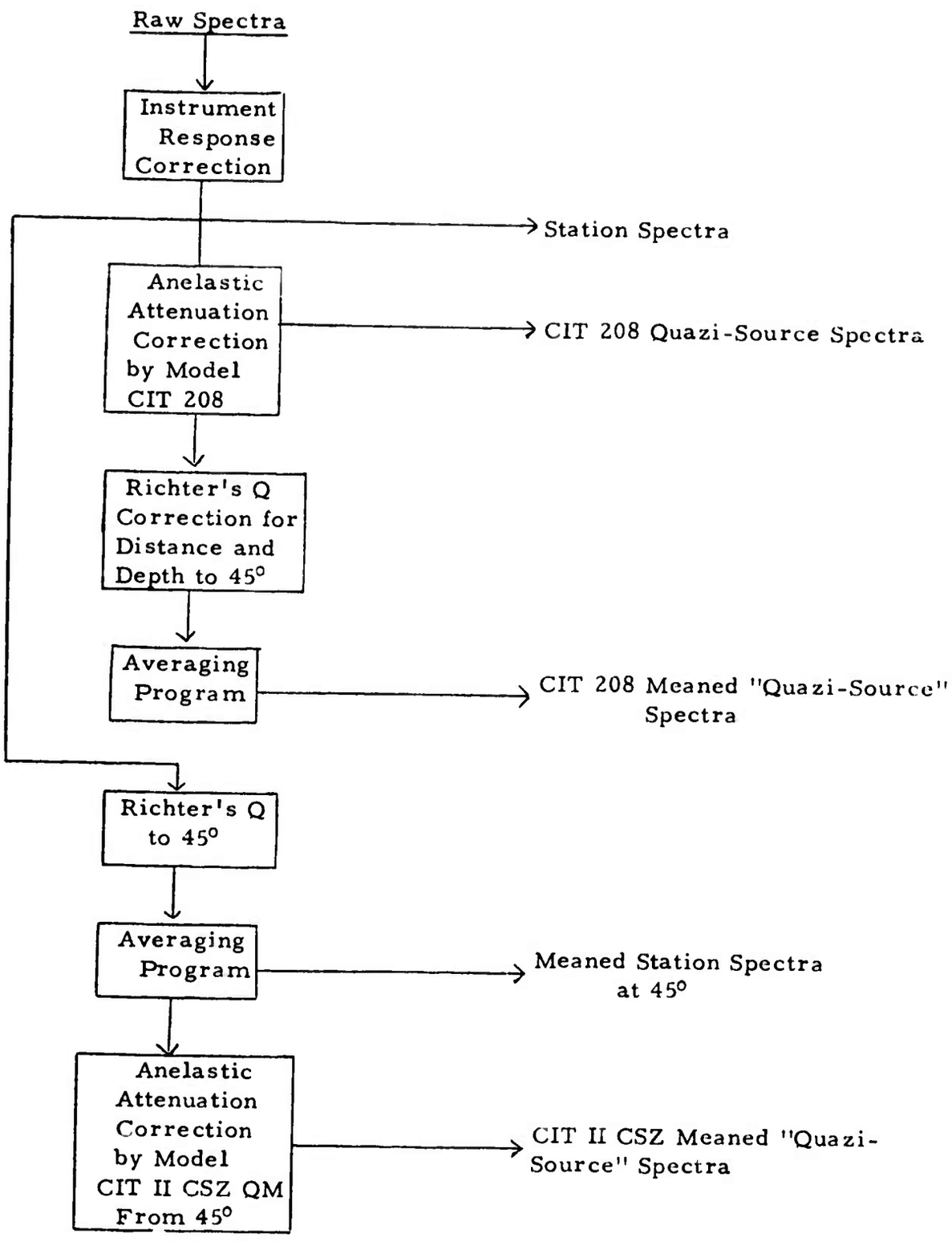


**Fig. 4.2**

Flow diagram relating raw spectra to meaned "quazi-source" spectra.

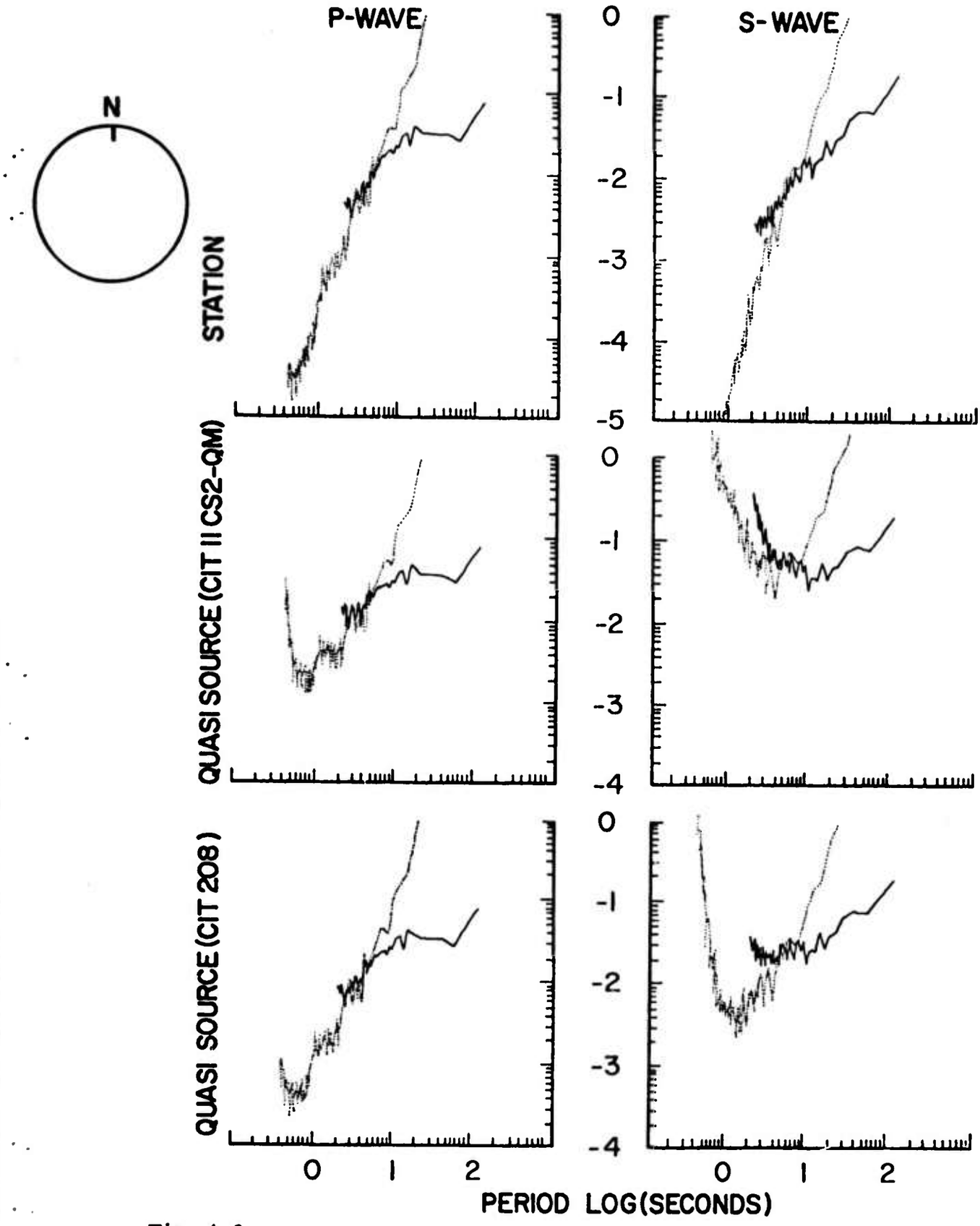


Fig. 4.3

Meaned spectra for event of February 11, 1969 in the Tien Shan region. Solid lines are long-period spectra. Dotted lines are short-period spectra. Each spectrum is an average over the number of stations indicated in Table II.

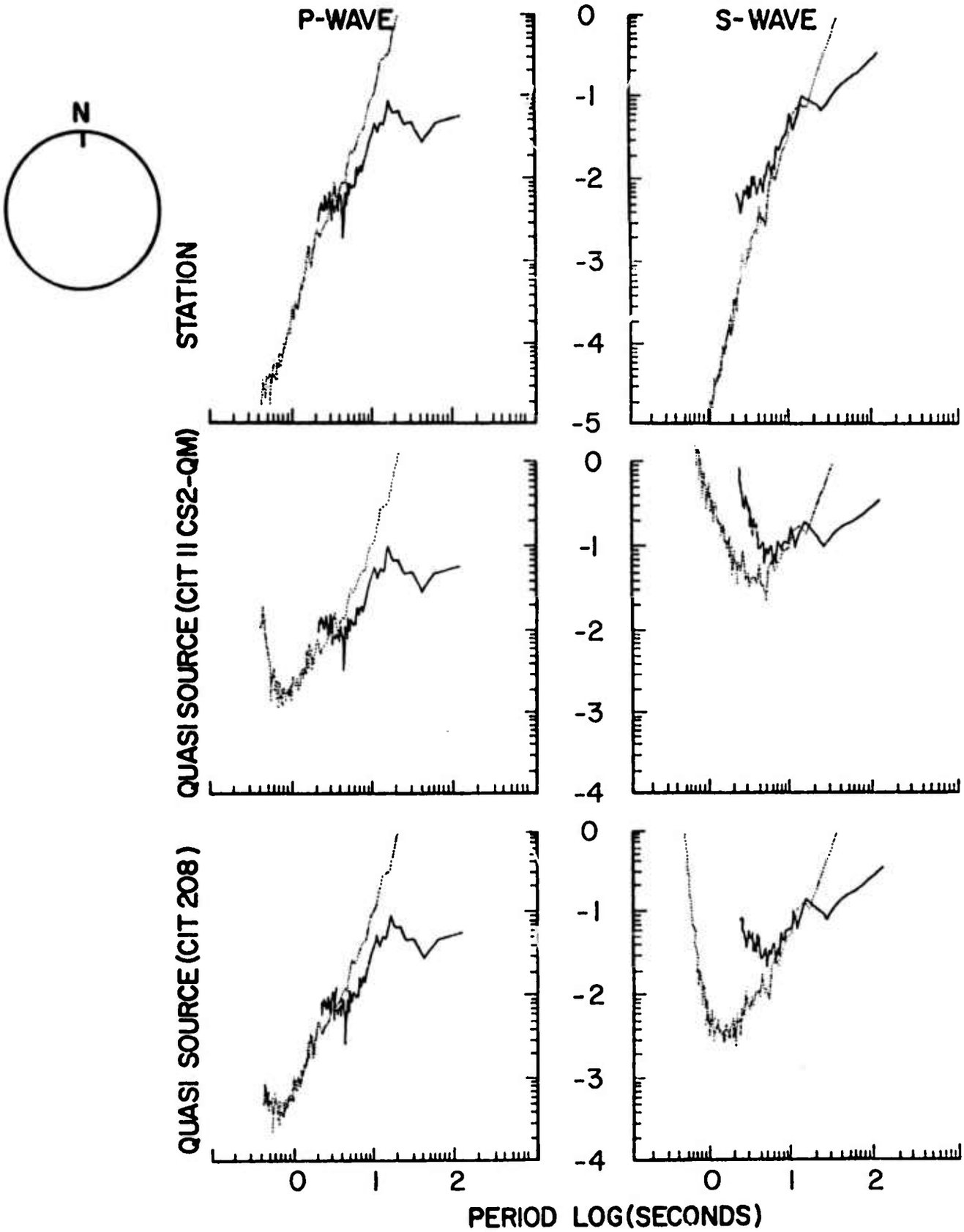


Fig. 4.4

Meaned spectra for event of June 5, 1970 in the Tien Shan region.

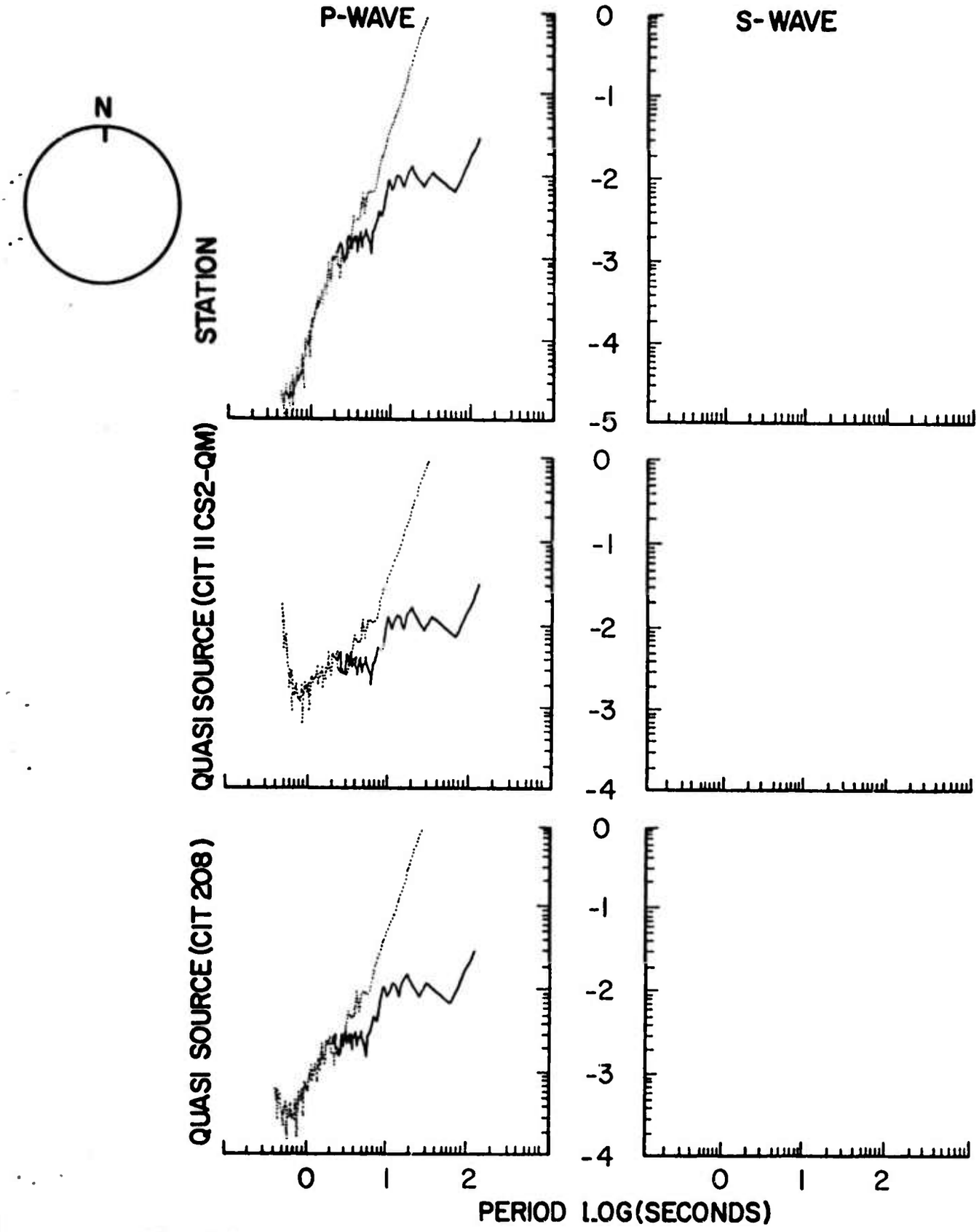


Fig. 4.5

Meaned spectra for event of March 23, 1971 in the Tien Shan region.

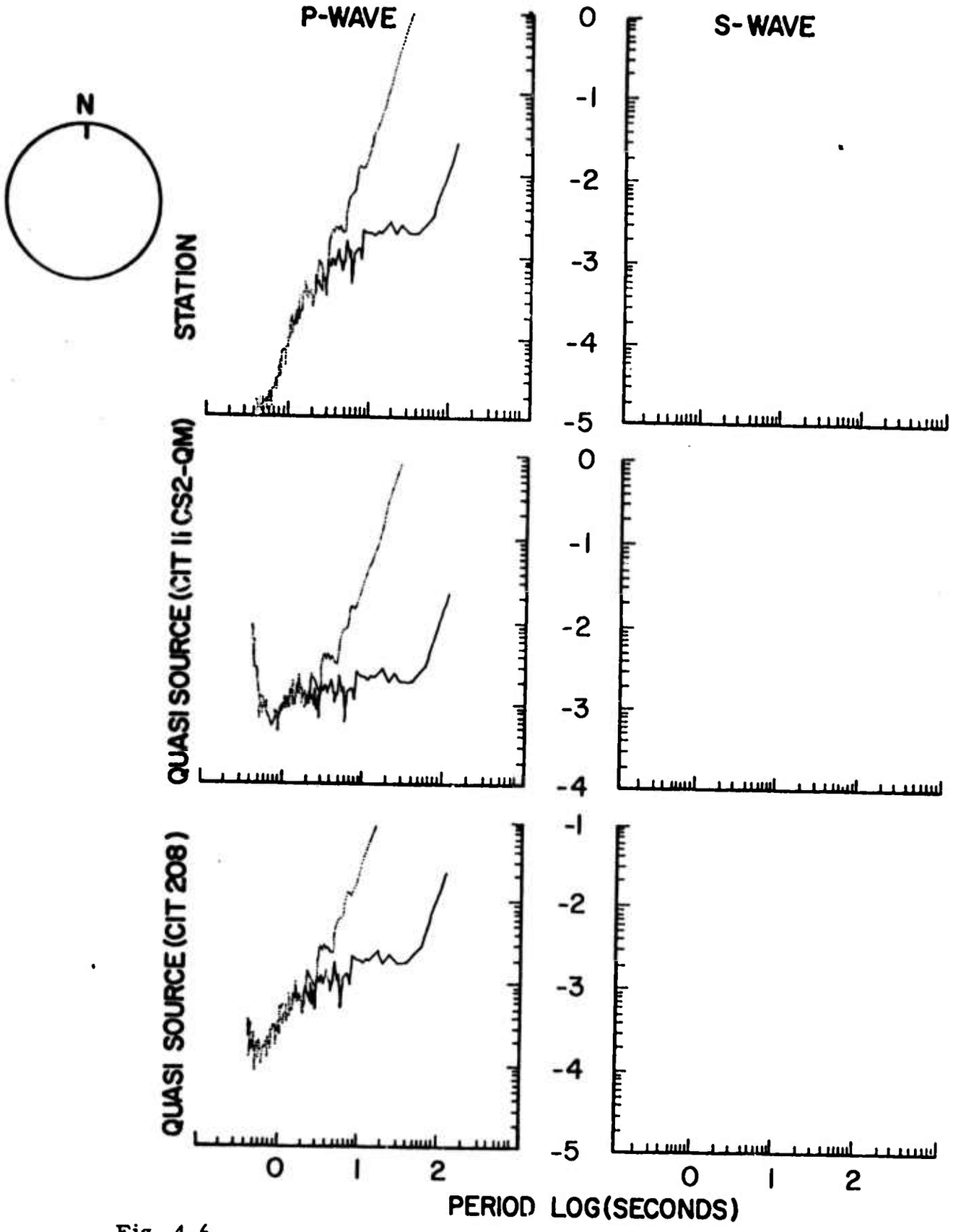


Fig. 4.6

Meaned spectra for event of April 9, 1972 in the Tien Shan region.

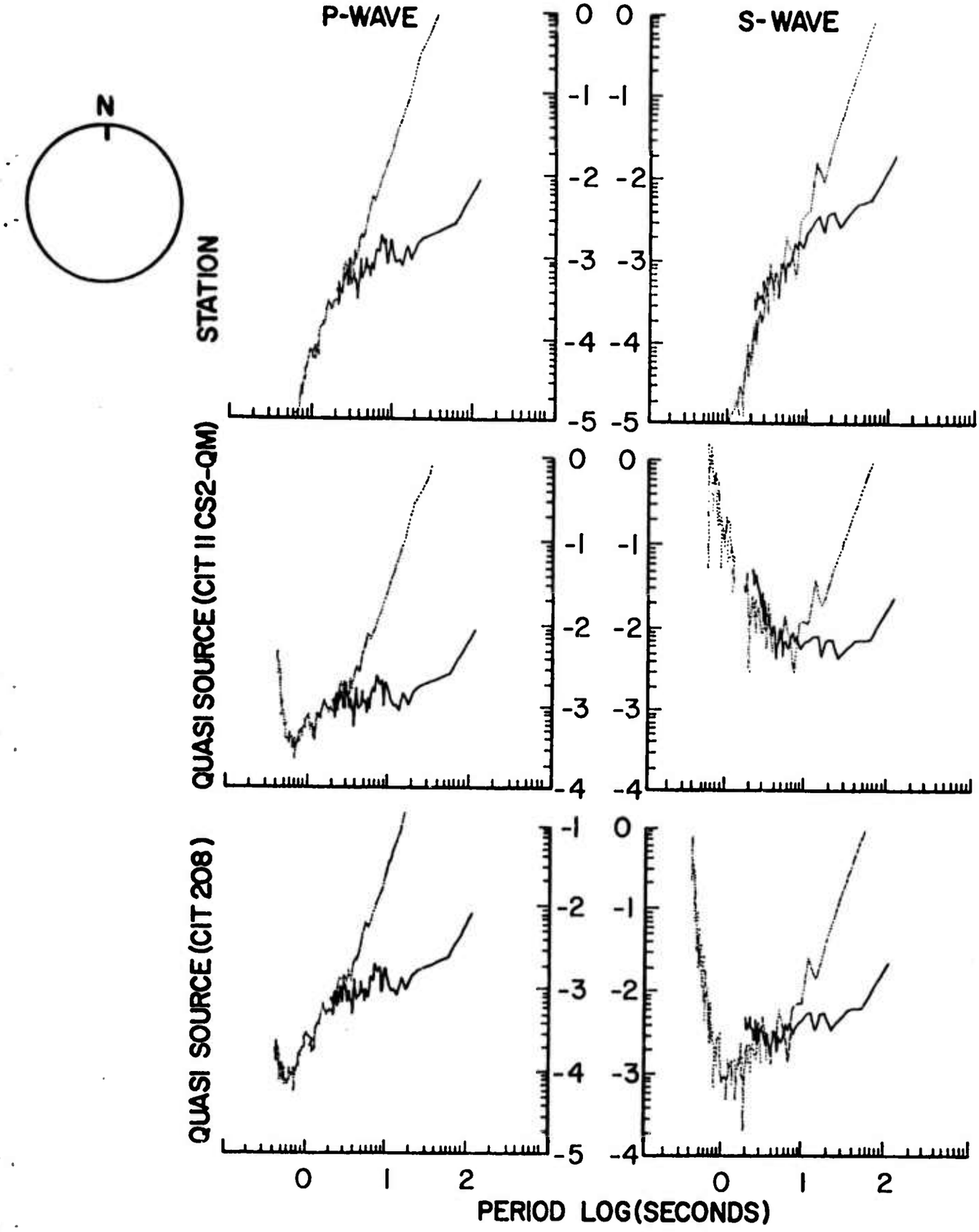


Fig. 4.7

Meaned spectra for event of August 15, 1967 in the Tibetan Plateau.

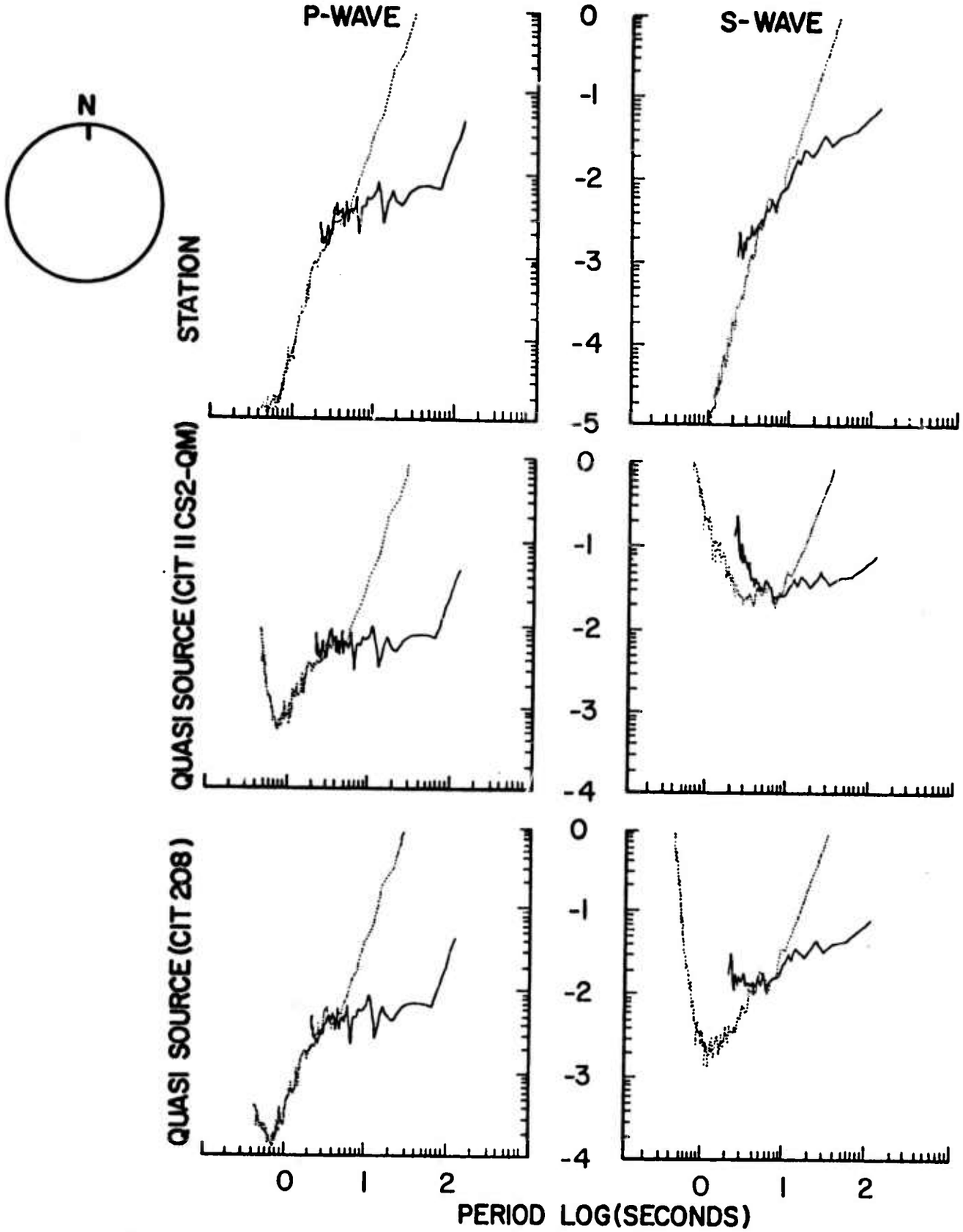


Fig. 4.8a

Meaned spectra for event of April 3, 1971 in the Tibetan Plateau. Short-period window about 60 seconds.

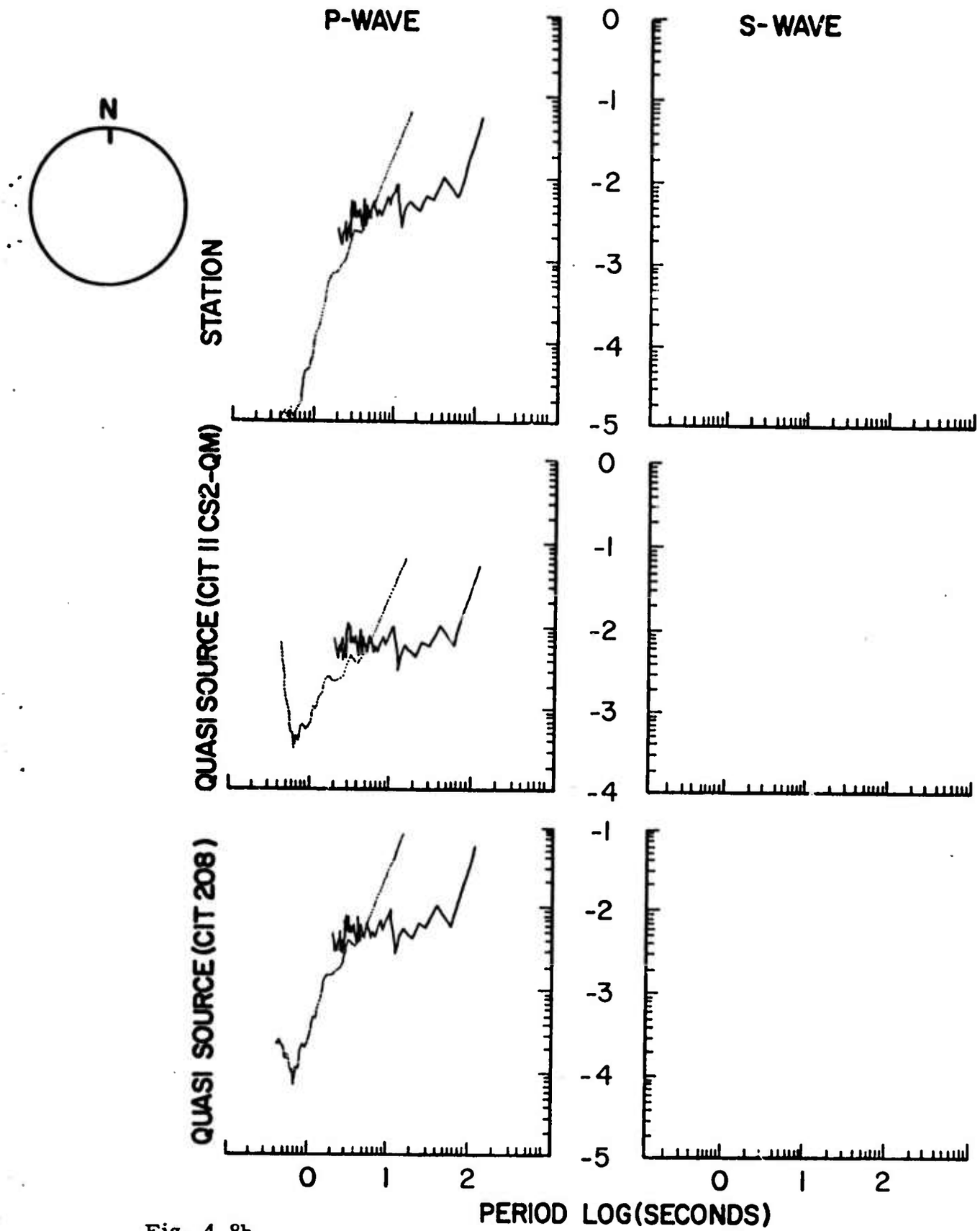


Fig. 4.8b

Meaned spectra for event of April 3, 1971 in the Tibetan Plateau. Short-period window about 20 seconds.

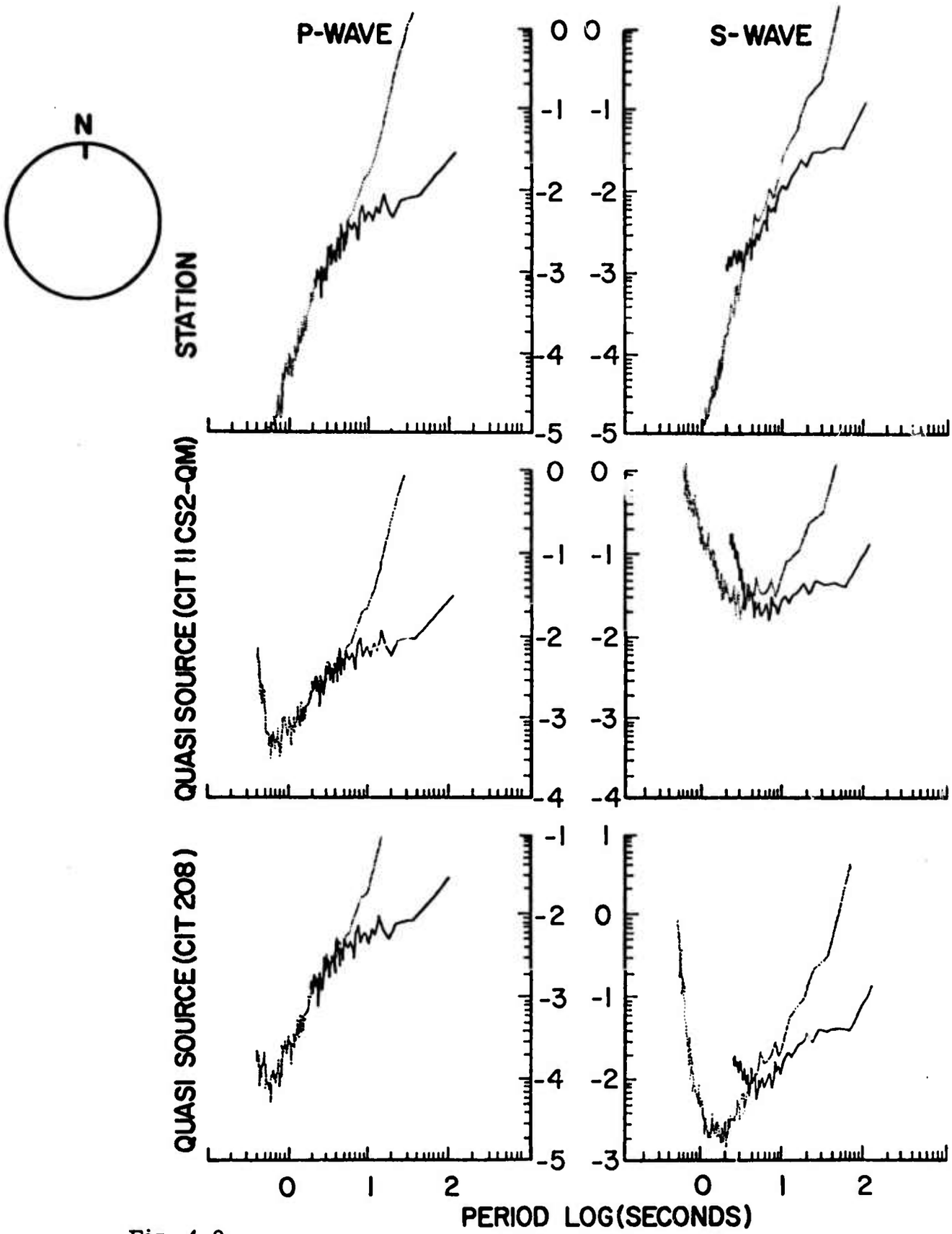


Fig. 4.9

Meaned spectra for event of May 22, 1971 in the Tibetan Plateau.

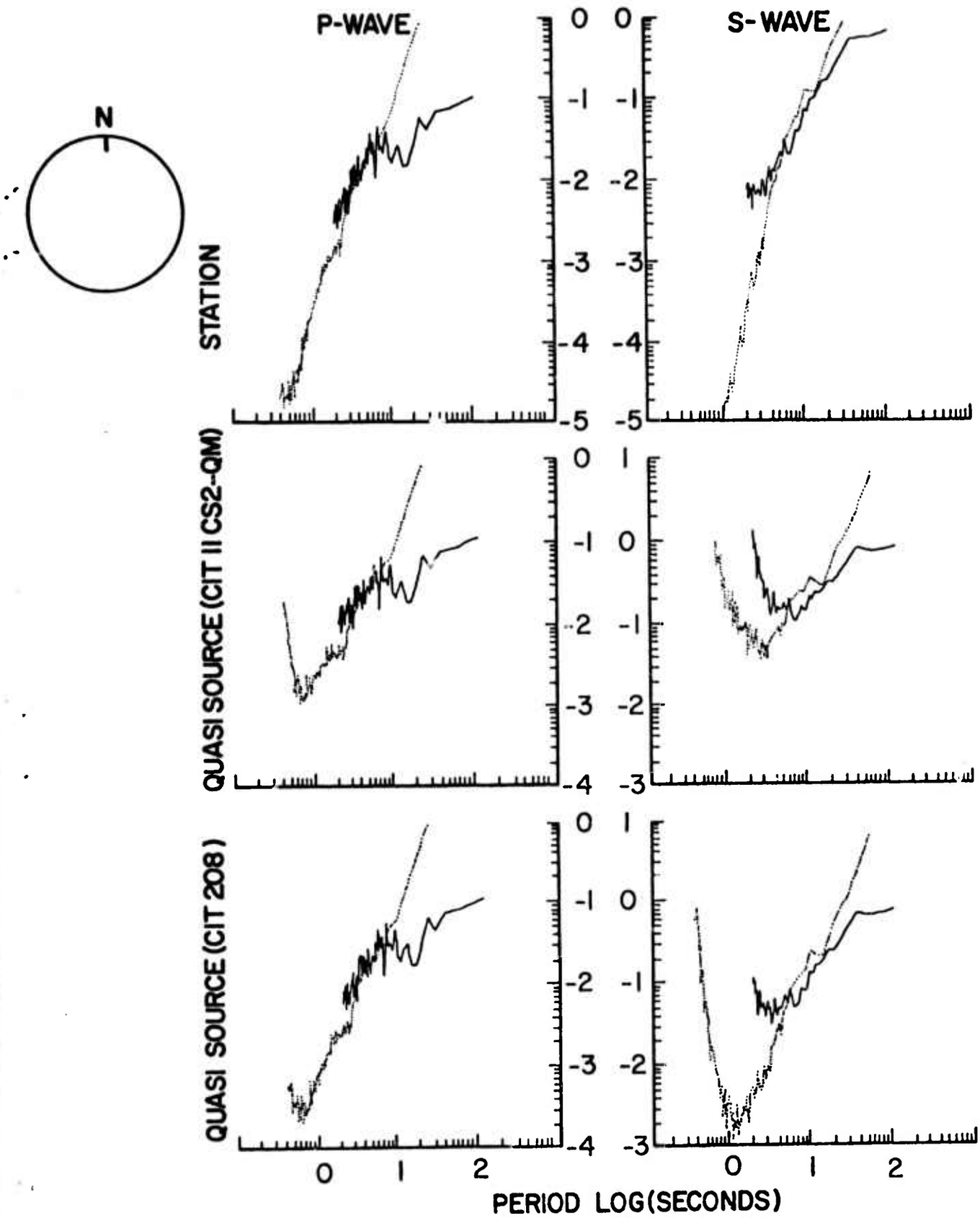


Fig. 4.10

Meaned spectra for event of April 19, 1963 in the Tsaidam Basin.

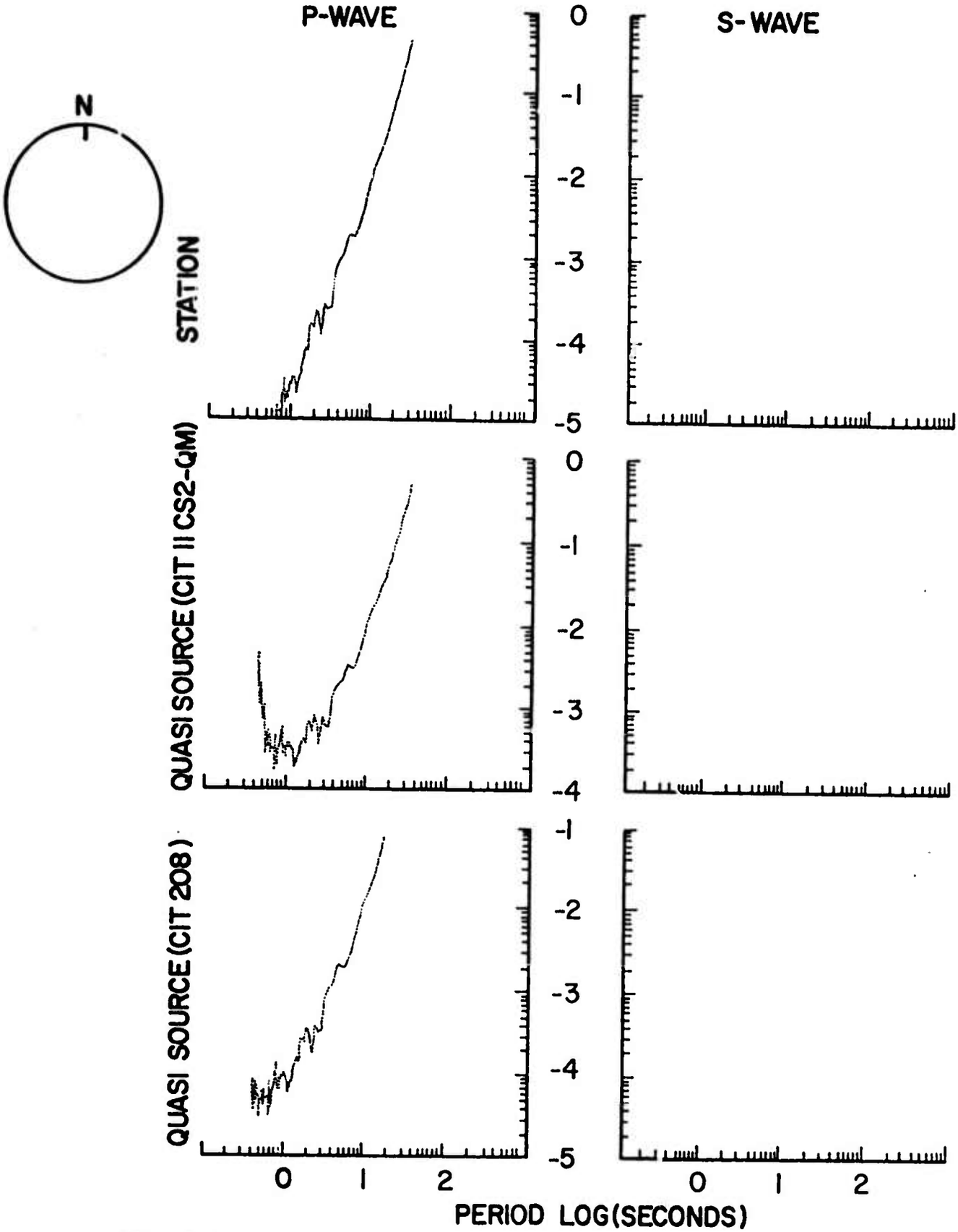


Fig. 4.11

Meaned spectra for event of February 11, 1967 in the Lake Baikal region.

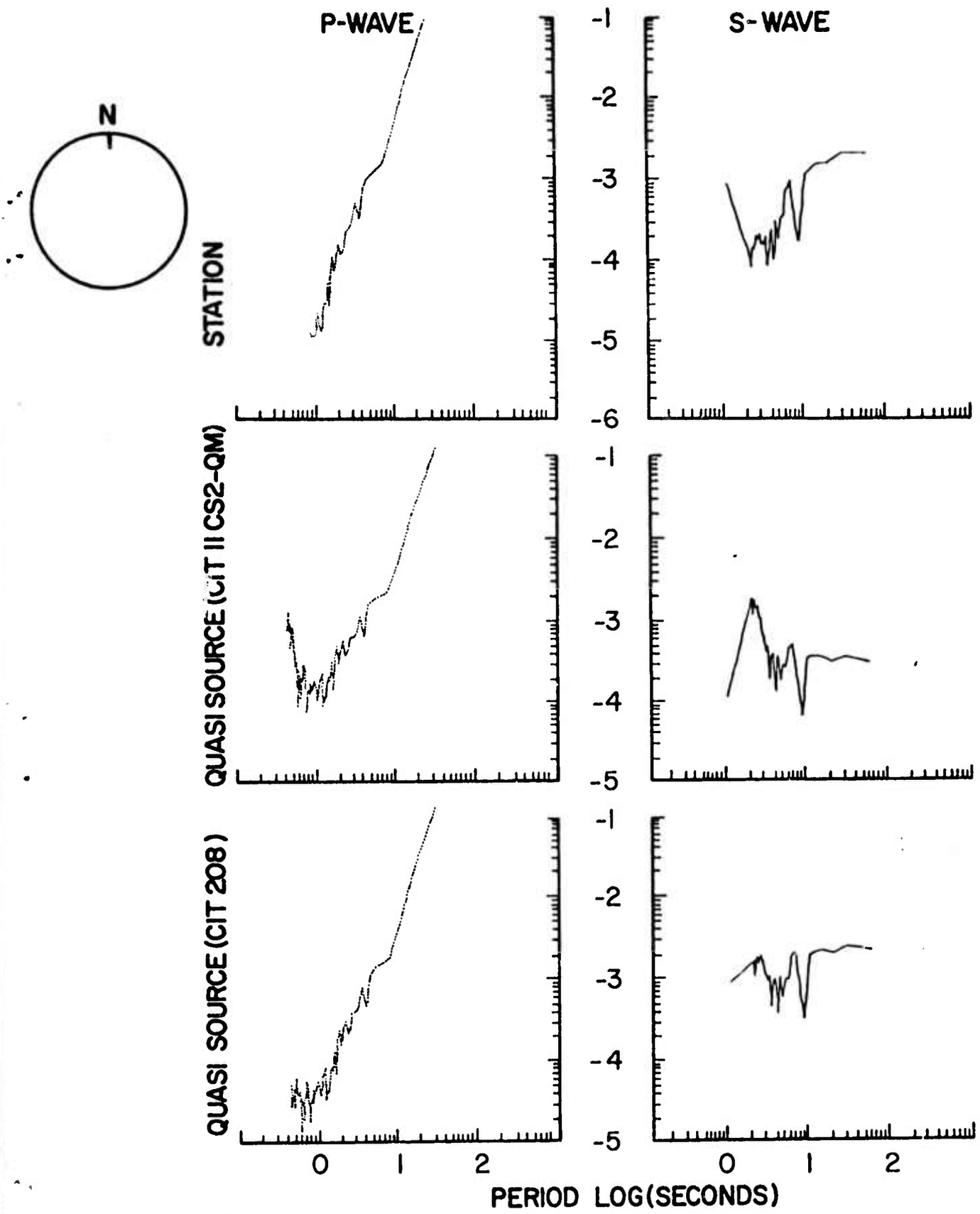


Fig. 4.12

Meaned spectra for event of March 28, 1970 in the Lake Baikal region.

correction according to CIT 11 CSZ QM is applied to the already meaned station spectra because the correction is virtually constant over the distance range of stations used.

Richter's Q is an empirical correction for distance and depth. All comparisons of spectra will be between spectra corrected to 45° by Richter's Q, yet corrected to the source for anelastic attenuation. This gives rise to the term "quazi-source" spectrum.

The spectra are averaged logarithmically rather than linearly. This method averages the shape of the spectra and avoids the problem of one spectrum dominating the average. This is equivalent, in terms of earthquake magnitude, to averaging the magnitudes from several stations, rather than averaging amplitudes.

Discussion.

Useable magnitudes have been computed for 13 events and $m_b$-Ms and $m_B$-Ms relationships have been compared to worldwide standards. Thus far no major deviations from worldwide relationships assembled by Ganse (1974) have been observed. Computed magnitudes are listed in Table II.

TABLE II

| Region | Date D | Date M | Date Y | Given Magnitudes MB | Given Magnitudes MS | Computed Magnitudes $m_b$ | Computed Magnitudes $m_B$ | Computed Magnitudes $M_s$ | Spectra SPP | Spectra LPP | Spectra SPS | Spectra LPS |
|---|---|---|---|---|---|---|---|---|---|---|---|---|
| Tien Shan | 04 | 05 | 65 | 5.7 | | Not | processed | | yet | | | |
| | 11 | 02 | 69 | 5.8 | | 6.15 (8) | 6.34 (7) | 6.38 (4) | (5) | (11) | (4) | (6) |
| | 05 | 06 | 70 | 6.0 | 6.6 | 6.17 (9) | 6.20 (9) | 6.67 (5) | (9) | ( 9) | (8) | (8) |
| | 23 | 03 | 71 | 5.7 | 6.8 | Not | processed | | yet | | | |
| | 23 | 03 | 71 | 6.0 | 6.9 | 5.93 (8) | 5.71 (8) | 5.91 (7) | (7) | (7) | All Radial | |
| | 09 | 04 | 72 | 5.9 | 5.3 | 5.73 (9) | 5.46 (5) | 5.43 (9) | (8) | (9) | All Radial | |
| | 02 | 06 | 73 | 5.8 | 5.6 | Not | processed | | yet | | | |
| Tibet | 15 | 06 | 65 | 5.6 | | 5.19 (13) | | 4.63 (8) | Too Small | | | |
| | 01 | 08 | 65 | 5.5 | | Too | Small | | | | | |
| | 15 | 08 | 67 | 5.7 | | 5.6 (26) | 5.48 (13) | 5.01 (19) | (12) | (4) | (2) | (6) |
| | 14 | 06 | 69 | 5.3 | | 5.07 (10) | 4.92 (1) | | Too Small | | | |
| | 03 | 04 | 71 | 5.7 | | 5.91 (34) | 5.84 (20) | 5.99 (38) | (12) | (7) | (7) | (11) |
| | 22 | 05 | 71 | 5.6 | | 5.85 (30) | 5.70 (16) | 6.04 (20) | (8) | (5) | (5) | (9) |
| | 22 | 07 | 72 | 5.5 | 5.8 | 5.49 (18) | 5.48 (8) | 5.48 (22) | In processing | | | |
| Tsaidam | 21 | 05 | 62 | | 7.13 | Data will be ordered from archives | | | | | | |
| | 19 | 04 | 63 | 5.4 | | 6.10 (24) | 6.36 (23) | 6.71 (18) | (10) | (9) | (6) | (8) |
| | 01 | 07 | 63 | 5.3 | | Too | Small | | | | | |
| | 16 | 03 | 64 | 5.9 | | Not | processed | | yet | | | |
| | 14 | 12 | 67 | 5.4 | | Not | processed | | yet | | | |
| | 24 | 03 | 71 | 5.8 | 6.4 | Not | processed | | yet | | | |
| | 30 | 08 | 72 | 5.5 | 5.3 | 5.22 (7) | 5.06 (5) | 4.99 (7) | In processing | | | |
| | 30 | 08 | 72 | 5.5 | 5.9 | 5.26 (7) | 5.04 (5) | 4.86 (7) | In processing | | | |
| | 16 | 06 | 73 | 5.4 | | Not | processed | | yet | | | |
| Lake Baikal | 15 | 01 | 67 | 5.2 | | Not | processed | | yet | | | |
| | 11 | 02 | 67 | 5.3 | | 5.15 (14) | | 5.16 (4) | (6) | | | |
| | 26 | 11 | 68 | 5.1 | | Not | processed | | yet | | | |
| | 28 | 03 | 70 | 5.2 | | | | | (6) | | | (3) |
| | 13 | 08 | 70 | 4.7 | | Unusable: Bad signal-to-noise ratio | | | | | | |
| | 09 | 08 | 72 | 5.1 | 4.7 | | | | In processing | | | |

Focal mechanisms have been computed for several events. All four events in the Tien Shan show thrust mechanisms with the pressure axis roughly normal to the trend of the Tien Shan mountains. These mechanisms are considered final, subject to very small changes based on Russian data. Mechanisms in the Tibetan Plateau are much more sketchy, but primarily strike slip motion. Four events yield an interpretation in which one fault plane is oriented nearly north-south and dipping steeply toward the East with left lateral motion. Two focal mechanisms for events beneath the Tsaidam basin are probably thrust-type with a north-south pressure axis. One mechanism for an event just south of the Tsaidam basin shows a strike-slip mechanism similar to those obtained for the Tibetan Plateau. One mechanism from Lake Baikal is primarily strike-slip. These mechanism types agree with published mechanisms for Asian earthquakes and will be updated with Russian data as that data becomes available.

The interpretation of spectra will be reserved for a later report. The size range and number of events is not sufficient at present to attempt an empirical scaling law for any individual region. As a brief characterization, spectra from the Tien Shan and Tsaidam show two well separated corners,

while, if two corners are interpreted on Tibetan spectra, they are very close. The three spectra from Tibet nearly overlay with small frequency shifts, while Tien Shan spectra are diversified in shape.

Some Russian seismograms have been digitized and spectra have been obtained. At this time, however, noticeable differences between corrected Russian spectra exist, implying an improper instrument correction. Though difficulties exist, the Russian data will make a great contribution. In particular, a few very low gain records have been found from which P spectra can be obtained for very near ($2^{\circ}$ - $5^{\circ}$) distances.

The limited amount of data available show that a spectral classification of Asian earthquakes is possible. Different spectra are observed for the Tien Shan and Tibet areas. Preliminary examination shows no correlation between spectral types and the distinctly different focal mechanism types.

References.

Anderson, D. L., Latest information from seismic observations, Chapter 12 in The Earth's Mantle (T. F. Gaskell, editor), pp 355-420, Academic Press, 1967.

Ganse R., A Study of Earthquake Magnitude and It's Relation to the Law of Seismic Spectrum Scaling, Ph. D. Thesis, St. Louis Univ., 1974.

Julian, B., personal communication.

Molnar, P., T. J. Fitch, and F. T. Wu, Fault Plane Solutions of Shallow Earthquake and Contemporary Tectonics in Asia, Earth and Planetary Letters, 19, 101-112, 1973.